LHCb 2000-102 Muon
24th October 2000

Beam tests of WPC-7 prototype of the wire pad chambers for the LHCb Muon System

B.Bochin, S.Guets, V.Lazarev, N.Saguidova, E.Spiridenkov, An.Vorobiev, A.Vorobyov.

Petersburg Nuclear Physics Institute.

Abstract

A new prototype of the Wire Pad Chamber for the LHCb Muon System, WPC-7, has been constructed at PNPI and tested in the T11 beam at CERN. This prototype proved to be more stable against the electrical discharges at high voltages thus extending the operational plateau of the chamber by 200V. This made it possible to operate with larger wire pad sizes up to 12x16cm^2. This report presents the results from the beam tests of the WPC-7 prototype: time resolution and efficiency, cross-talk, noise counting rates, streamer probability measured at various high voltages and discriminator thresholds.

Contents

1 Introduction.

In our previous Note [1], we presented a description of the double-gap wire pad chambers (WPC) proposed for the LHCb Muon System together with the results of the beam tests performed in the T11 beam at CERN. Several WPC prototypes constructed at PNPI have been tested. These tests demonstrated that the detection efficiency of a double gap WPC with the wire pad sizes up to 64 cm^2 proved to be better than 99% (25 ns time window) within a 300 V plateau while operating with the $Ar/CO_2/CF_4$ gas mixture. The time resolution and efficiency were practically independent on the beam inclination ($0<\Theta<200$ mr) and on the beam rates up to 500 kHz per channel. The cross-talks were quite small: the probability to fire the neighbouring pads was about 2% at the nominal HV=3.15 kV.

Though these results were considered as satisfactory, still it would be desirable to increase the efficiency plateau that would give it possible to operate with larger pad sizes and to provide more redundancy in the chamber performance.

One attempt to extend the plateau was described in the above mentioned Note [1]. It was demonstrated that replacement of the CF_4 component in the $Ar/CO_2/CF_4$ gas mixture by $C_2H_2F_4$ increased considerably stability against the electrical discharges in the chamber volume thus extending the operation plateau by more than 200 V. In particular, it was shown that the 99% efficiency in a 25 ns window could be reached within a 400 V plateau with the pad size of 128 cm^2. These results looked very promising. However, further studies at PNPI (to be published) showed that the $Ar/CO_2/C_2H_2F_4$ gas mixture has very poor ageing properties, and therefore it can not be recommended for application in the LHCb Muon System operating in hard radiation environment . On the contrary, the $Ar/CO_2/CF_4$ gas mixture provides outstanding stability of the MWPC operation at very high radiation dozes. This was demonstrated first in the local [2] and more recently in the global (to be published) ageing tests performed at GIF with the CMS chambers having design similar to that of the described here WPC. So, the $Ar/CO_2/CF_4$ gas mixture remains the best candidate for the LHCb muon chambers.

Fortunately, the new WPC prototypes constructed at PNPI proved to be essentially more stable against the discharges. With the $Ar/CO_2/CF_4$ gas mixture, they were able to operate up to HV_{max}=3.45 kV instead of

HV_{max}=3.25 kV reached with our previous prototypes thus extending the efficiency plateau by 200 V. These prototypes have been tested in the T11 beam at CERN in April-May 2000. One of them (WPC-6) contained, in addition to the wire pads, two rows of cathode pads of various sizes. The other one (WPC-7) contained only wire pads. Both prototypes had sensitive areas of 16x24 cm^2.

Here we report on the test results obtained with the WPC-7 prototype.

2 Design of WPC-7 prototype.

The design of the double-gap WPC-7 prototype was nearly identical to the design of the WPC-1m prototype described in [1]. Figure1a shows a schematic view of the chamber. The chamber has a rectangular shape with the sensitive area of 16x24 cm^2. The wires are wound along the short side and grouped together to form four pads of 4x16 cm^2 and four pads of 2x16 cm^2 size. Our goal was to study performance of the WPC with larger pads. Therefore, several pads were joint together electrically to form only three pads: W1(4x16 cm^2), W2(8x16 cm^2), W3(12x16 cm^2) as shown in Figure 2. The main parameters of WPC-7 are as follows:

Gap between the cathodes : two gaps, 5.00 mm each
Anode wire spacing : 1500 μm
Anode wire diameter : 30 μm
Anode wire tension : 30g.

One side of each wire pad was connected to a common HV bus through a 2MΩ resistor. The other side of each pad was connected through a 1000 pF decoupling capacitor and a diode protection circuit to a preamplifier. All cathode planes were grounded. The external Cu-plates were also grounded providing additional shielding of the chamber.

3 Electronics.

The WPC-7 prototype was equipped with the PNPI front-end electronics based on discrete elements and consisting of a preamplifier followed by a

main amplifier. This electronics was similar to that used in our previous tests [1]. The only difference was a slightly higher (by 20%) amplification factor. The input impedance of the preamplifier was 30 Ω plus a 20 Ω contribution of the double R-diode protection circuit. Each channel contained a fast (F) and a slow (S) outputs. The signal shaping was optimised for detection of the chamber current $I(t) \propto (t+t_0)^{-1}$ with t_0=1.87 ns.

The calculated sensitivities of the channels are as follows:

Sensitivity (F-channel) : 5 mV/fC at C_{in} = 50 pF,
2.5 mV/fC at C_{in} = 200 pF.

Sensitivity (S-channel) : 2 mV/fC at C_{in} = 50 pF,
1.5 mV/fC at C_{in} = 200 pF.

The calculated equivalent noise charge is:

σ_n (F-channel) = 1250e + 50 e/pF,
σ_n (S-channel) = 1870e + 20 e/pF.

Here, C_{in} is the total input capacitance.
C_{in} = 110 pF (4x16 cm^2 pad),
C_{in} = 200 pF (8x16 cm^2 pad),
C_{in} = 290 pF (12x16 cm^2 pad).

The signals from the F-channels of the Main Amplifier were sent to the leading-edge discriminators (Le Croy 4416B) with adjustable thresholds, and the output signals from the discriminators were used to measure the arrival time of the signals (16-bit TDCs ,Le Croy 1176). The current signals from the S-channels integrated in a 80 ns time window at the input of the 14-bit ADCs (Le Croy 1182) provided information on the detected charge.

4 Experimental setup.

The WPC-7 prototype was tested at CERN in a 3 GeV/c negative pion beam at PS. The layout of the experiment is shown in Figure 3. Beam particles were detected with two scintillator counters: S1 (15cmx15cm) and

S2 (20cmx20cm). The coincidence between these two counters in a 10ns window provided a trigger signal:

$$TR1 = S1xS2.$$

The constant-fraction discriminators (CFD) were used in both S1 and S2 channels helping to reduce the time jitter of the trigger signal down to ≤1ns. The beam particles were detected also by two planes (H – horizontal and V - vertical) of the hodoscope counters, each plane containing 8 counters (1cmx8cm). The following information was registered by the acquisition system:

- Time arrivals and amplitudes of the signals from S1 and S2 scintillator counters measured with TDCs and ADCs.
- Time arrivals of the signals from all hodoscope counters measured with TDCs.
- Time arrivals of the signals from the WPC F-channels measured with TDCs.
- Integrated current signals from the WPC S-channels measured with ADCs.

In addition, there was ungated data from the scalers detecting signals from all scintillator counters and from the WPC F-channels. The scalers provided two types of information: the total number of counts during the beam spill and the number of counts during a 330 ms interval in-between the beam spills. The beam spill was around 330 ms.

The WPC was installed on a movable platform allowing to vary the beam position over the chamber area. A premixed gas mixture from a bottle was used in these tests. The gas mixture was $Ar(40\%)+CO_2(50\%)+CF_4(10\%)$. This was the same gas mixture as used in the aging tests of the CMS CSCs at GIF. The data taking was performed in the period from 12.05.2000 to 17.05.2000. In all these measurements, the beam intensity was around $5 \cdot 10^4$ particles per spill. The beam size was about 5 cm in diameter.

5 Data analysis and results.

Figures 3a, 3b display the average shapes of the signals from the smallest and the largest pads W1 ($4x16cm^2$) and W3 ($12x16cm^2$), as recorded with a digital oscilloscope at the output of the Main Amplifier.

The main parameters of the measured signals are presented in Table1. Figure 3c displays a signal event from pad W3 ($12x16cm^2$) detected in a

larger time interval showing the quality of the tail cancellation and also the noise levels in the Fast and Slow channels.

Pad	Pad size cm^2	Channel	Rise time ns	FWHM ns	Width (10%) ns	Width (5%) ns
W1	4x16	Fast Slow	14 18	33 39	65 72	78 82
W3	12x16	Fast Slow	16 20	36 42	70 78	85 90

Table 1. Main parameters of the averaged signals from pads W1 and W3 at the output of the Main Amplifier.

Shown in Table 1 rise time is the time interval during which the signal increases from 10% to 90% of its amplitude. Also shown are the full width at half maximum (FWHM) and the width of the signals on a level of 10% and 5% of the amplitude.

The ADC and TDC spectra of the signals from the WPC S-channels and F-channels, respectively, were measured in these tests. The events were selected after several cuts applied to the raw data from the beam defining scintillator counters and the hodoscope:

- Cut1. Shower rejection.

  Large amplitudes in the ADC spectra from the S1 and S2 counters were rejected. The pile-ups of two and more particles in the 20ns time window were rejected in this way. Typically, about 10% of the events were rejected by this cut. The remaining events were considered as TR2-events.
- Cut2. Hodoscope selection.
  - Only signals in a 20 ns time window in the TDC spectra were selected.
  - There should be one and only one signal both in the H-plane and in the V-plane of the Hodoscope. This helps to kill further the showers in the beam.

– A certain combination of the hodoscope counters could be selected to define a beam spot.

The events passing Cut1 and Cut2 were considered as TR3-events. No cuts have been applied to the signals from WPC.

The number of the TR3-events was used in calculations of the efficiencies in the S- and F-channels of WPC:

$$Eff_{ADC} = \sum_{i=350}^{overflow} N_i(ADC) \Big/ \sum TR3 \qquad (1)$$

$$Eff_{TDC} = \sum_{t1}^{t1+\Delta t} N_i(TDC) \Big/ \sum TR3 \qquad (2)$$

Figures 4 to 6 present some examples of the TDC and ADC spectra of the signals from pad W2 (8x16 cm^2) at the nominal HV=3.15kV and also at HV=3.05kV and HV=3.30kV. The discriminator threshold was set at 35mV in these measurements.

The pedestal in the ADC spectra was in channel 260 with a spread of 18 channels.

The hodoscope selection guaranteed that at least 99% of the selected particles were inside the pad size. This value was controlled by the ADC efficiency determined according to expression (1).While filling the TDC histogram, at least one hit in the time window from 240 ns to 290 ns was required. When more than one hit were observed in this window, only one of them (first arrival) was included in the histogram. However, the frequency of such double-hit events was quite low (<1%). Note that the time direction in the TDC spectra in Figures 4-6 goes from the right to the left side. From the time distributions, the following quantities were obtained: mean time, r.m.s., and the registration efficiencies in various time windows (50 ns, 25 ns, 20ns, 15 ns) according to expression (2).

5.1 Noise counting rates.

As it was mentioned above, the noise counting rate was measured between the beam spills with the ungated scalers at the outputs of the discriminators in the WPC F-channels. The results of the measurements for various pads and various thresholds are presented in Figure 7. One can see

from this figure that the counting rates are quite low at HV≤3.2kV and Th≥35mV, most of the rate being due to the physical background (cosmic muons etc). The contribution of the noise starts to be visible at the Th=26 mV, and it proved to be more essential for smaller pads (W2 and, especially, W1). In fact, the pure electronics noise in these channels is even smaller than in the W3 channel. The observed counting rates are explained by the contribution of the pickup noise, which happened to be larger for smaller pads. Hopefully, this noise can be eliminated in future by better screening/grounding.

With increase of the high voltage beyond HV = 3.2 kV, the noise counting rates smoothly increase. After HV = 3.4 kV the increase becomes more sharp, and some fluctuations of the noise rates appear. Still the chamber operated at HV = 3.45 kV without noticeable dark currents. The beam initiated trips were observed only at HV = 3.5 kV.

5.2 Time resolution and efficiency.

Figures 8a to 13a demonstrate the time resolution (r.m.s) and efficiency determined from the time distribution similar to those shown in Figures 4-6. The measurements have been performed for various discriminator thresholds from Th = 26 mV to Th = 45 mV.

We assume that the requirements of the LHCb experiment are satisfied if the efficiency in the 20 ns window exceeds 95%. This determines the lowest HV_{min}, while the highest HV value is determined by appearance of the sparks and dark currents in the chamber. In the WPC-7 prototype, this limit proved to be HV_{max} =3.45 kV. Taking into account the high uniformity of the gas gain (±20%) in the designed WPCs, we consider that the nominal HV value might be chosen as $HV_{nom}= HV_{min}$ +100V. Note that the change of HV by 150 V leads to a change in the gas gain by a factor of 2. The time resolution (r.m.s) proved to be around 5 ns at HV_{min}, 3.5 ns at HV_{nom} approaching 2.0÷2.5 ns at HV_{max}.

Table 2 presents the HV_{min} values obtained for various pads and thresholds. Also presented is the length of the plateau determined as the difference HV_{max} - HV_{min}.

Pad	Pad size cm^2	Thresh mV	HV_{min} kV	Plateau V
W1	4x16	26	2.92	530
W1	4x16	35	2.97	480
W1	4x16	45	3.02	430
W2	8x16	26	3.0	450
W2	8x16	35	3.05	400
W3	12x16	26	3.05	400

Table2. Efficiency plateau for various pads and thresholds.

One can see that, though the efficiency plateau decreases with the increase of the pad size, still it remains quite large (400 V) even for the largest pad W3 that is 190 cm^2 in size. The plateau is larger for lower thresholds. The minimal threshold is determined by the noise level. In the present noise conditions, the preferable threshold is Th=35 mV for the W1-channel, and it can be as low as Th=26 mV for the larger pads W2 and W3. Note that the gas gain depends on the atmospheric pressure: 1% decrease in the atmospheric pressure leads to 7% increase in the gas gain. All presented here measurements were performed at quite high atmospheric pressure of 1030mbar.

Figure 14 shows the dependence on HV of the mean time of the time distributions for various pads and thresholds. One can see the typical for the leading-edge discriminator dependence of the mean time on HV and on the threshold level. The time walk increases with the increase of the pad size. The main contribution to the time walk comes from the small amplitude region. This is illustrated by Figure 15 showing the TDC mean time and r.m.s. determined for various ADC zones (pad W2, nominal HV=3.15 kV). The mean time in the ADC zone 1 deviates by 6 ns from the average. Also, r.m.s. becomes much worse in this zone. Note, however, that only about 10% of the events populate zone 1 at the nominal HV=3.15 kV. That is why the total time resolution and the efficiency are not much deteriorated by the contribution of this zone.

In all presented above illustrations, the threshold levels were given in terms of mV. It is possible also to relate the threshold levels with the collected charge. This was done by analysing the ADC spectrum at low HV=2.9 kV where the spectrum starts from quite low amplitudes, some of them being below the discriminator threshold level. Figures 16a and 17a show this spectrum for pad W2 ($8x16cm^2$) without selection in the TDC channel and also after requiring appearance of the signals in the 30 ns time window. The ratio of these counting rates gives the efficiency of the TDC channel as a function of the amplitude in the ADC channel. Figures 16b and 17b demonstrate this efficiency, Eff_{TDC}, for Th=26 mV and Th=35 mV, respectively. The signal amplitude in the F-channel becomes equal to the discriminator level when Eff_{TDC} = 50%. As it follows from Figures 16b and 17b, this happens when the charge measured with the ADC is around channels 260 and 370 for Th=26 mV and Th=35 mV, respectively, the ADC pedestal (250 ch) being subtracted. These values should be compared with the ADC_{mean}≈2500ch at the nominal HV=3.15 kV. We conclude from this comparison that, at the nominal HV=3.15 kV, the threshold levels Th=26mV and Th=35 mV correspond, respectively, to ≈10% and ≈15% of the mean ionization charge (≈100e in our case) deposited in the WPC. Note, however, that the collection time of the ionization electrons in WPC is about 30 ns, therefore, only part of them (≈30%) arrive on the anode wires before the discriminator is triggered. If all ionization electrons were collected on the anode wire simultaneously, in this case the thresholds 26 mV and 35 mV would correspond approximately to arrival of the 4-th and the 6-th electrons, respectively.

5.3 Cross-talks.

An important requirement to the muon chambers in the LHCb Muon System is quite strong limitation on the pad cluster size. It should not exceed 1.2 in the operational region of WPC (in our case in the region of ±100 V around $HV_{nominal}$). This means that the cross-talks between the neighbouring pads and, especially, between the non-neighbouring pads should be as low as possible. To measure the cross-talks between various pads, we selected with the beam hodoscope the beam spot to be inside one certain pad and detected signals appearing in the other TDC channels in the time interval $0 \le t \le 300$ns. A small correction was applied taking into account signals due to real

particles crossing these pads. This was done by subtracting the signals exceeding channel 800 in the corresponding ADC-channel. So the cross-talks probability was determined according to the following expression:

$$cross-talk = \frac{(\sum_{0}^{300} TDC - \sum_{800}^{over} ADC)observed\_pad}{(\sum_{250}^{300} TDC)in-beam\_pad} \qquad (3)$$

Thus obtained cross-talk probabilities for various pad combinations and various discriminator thresholds are presented in Figures 8b to 13b. One can see from these figures that the cross-talk between the non-neigouring pads (W1→W3, W3→W1) is neglegible even at the highest HV-values.

The cross-talk between neighbouring pads depends on the discriminator threshold and on the HV – value.

Observed pad	In-beam pad	Thresh mV	HV_{nom} kV	Cross-talk, %	
				HV_{nom}	HV_{nom} +100V
W2 8x16 cm^2	W1 W1 W1 W3	26 35 45 26	3.10 3.15 3.20 3.10	5.0 3.6 5.0 1.9	8.9 7.7 9.4 2.9
W1 4x16 cm^2	W2 W2	26 35	3.02 3.07	1.5 1.7	3.2 2.9
W3 12x16 cm^2	W2 W2	26 35	3.15 3.20	3.4 1.5	6.7 3.3

Table3. Cross-talk probabilities for various combinations of the pads and various discriminator thresholds.

Table3 presents the cross-talk probabilities for the nominal HV – values corresponding to the observed pads at a given discriminator threshold and also for HV_{nom} +100 V. One can see from this table that, in the nominal conditions, the cross-talk probability does not exceed 5%. It is interesting to note also that the cross-talk from a larger pad to a smaller pad proved to be less than in the inverse direction at the same HV – values and the discriminator thresholds:

$$\textit{Cross-talk (W2}\rightarrow\textit{W1)} = \begin{cases} \textit{2.9\% (HV=3.10 kV, Th=26 mV)} \\ \textit{1.7\% (HV=3.15 kV, Th=35 mV)} \end{cases}$$

$$\textit{Cross-talk (W1}\rightarrow\textit{W2)} = \begin{cases} \textit{5.1\% (HV=3.10 kV, Th=26 mV)} \\ \textit{3.6\% (HV=3.15 kV, Th=35 mV)} \end{cases}$$

$$\textit{Cross-talk (W3}\rightarrow\textit{W2)} = \textit{2.6\% (HV=3.15 kV, Th=26 mV)}$$

$$\textit{Cross-talk (W2}\rightarrow\textit{W3)} = \textit{3.4\% (HV=3.15 kV, Th=26 mV)}$$

Considering the cross-talk probability as a function of the signal amplitude, we see that practically all cross-talk signals are due to events with overflow in the ADC channel of the in-beam pad (Figure 18). Another way to see the effect of the cross-talk is observation of the shifts of the ADC pedestals in the neighbouring channels for various amplitudes in the ADC channel of the in-beam pad (Figure 18). Although the shifts start to be visible already for the ADC zones 2, 3, and 4, still the drastic changes appear only for zone 5 (overflow in the in-beam pad ADC), as illustrated by Figure 19b. Figure 19c shows clear correlation of the cross-talk signals in the TDC-channel with appearance of large amplitudes in the ADC-channel.

5.4 Cluster size.

The pad-to-pad cross-talk discussed in the previous section leads to appearance of pad clusters fired by a beam particle. In addition, there might be “physical” clusterisation due to beam particles crossing the chamber at the border of two pads. Direct measurements of the cluster size were performed with the beam profile centred in the region between the pads W2

and W1 (Figure 20a). Figure 20b shows the cluster size for various positions of the beam spot selected by the beam hodoscope counters. One can see some slight increase of the cluster size near the pads border. Note, however, that these results were obtained with the chamber oriented perpendicular to the beam direction. Also, the width of the hodoscope counters was quite large (1cm). Figure 21 presents the yields of single, double, and triple clusters vs HV obtained from measurements with a "wide beam" (same beam profile as in Figure 20a but defined by ORing all hodoscope counters). From this figure one can see that the probability for SINGLES remains above 93%, and the probability of the triple clusters is below 0.3% in the designed operational region (HV ≤ 3.25 KV).

5.5 **Streamer probability.**

A special run with the gain of the Main Amplifier reduced by a factor of 20 was performed in order to see the signals considerably exceeding the nominal Landau distribution. Indeed, several such signals (16 in total per 12450 events) were observed as overflows in the ADC spectrum with an empty region between the ADC channels 2000 and 4000 (Table 4).
It was checked that all overflow signals are strictly correlated with the incident particles being in the 25 ns time window in the TDC spectra. In these measurements, the beam was focused on pad W3 ($12x16cm^2$), and the chamber operated at HV=3.15 kV. If we interpret the overflow events as the streamers, then we should conclude that the streamer probability is 0.13% in the WPC operating at HV=3.15 kV. There was no indication observed that the appearance of such signals deteriorates the normal performance of WPC.

ADC region, channels	counts
200-400	11586
400-1000	807
1000-1500	34
1500-2000	7
2000-4000	0
overflow	16

Table4. ADC distribution of the signals from pad W3 with reduced gain of the Main Amplifier.

6 Summary.

The constructed at PNPI prototype WPC-7 of the double-gap wire pad chambers has been tested in the T11 pion beam at PS. The prototype was equipped with the PNPI FE electronics, and it operated with the nominal gas mixture: Ar(40%)+CO_2(50%)+CF_4(10%). The prototype demonstrated stable operation in a wide high voltage range, thus extending considerably the efficiency plateau if compared with the previous prototypes described in [1]. In WPC-7, the efficiency plateau reached 500V for wire pads of 4x16cm^2 size and 400V for wire pads of 12x16cm^2 size. At the nominal high voltage defined as HVmin+100V, the performance parameters were as follow:

- efficiency in 20 ns time window > 98%;
- time resolution - 3.5 ns (r.m.s.);
- cluster size - 1,06;
- noise counting rate ≈ 0,1 Hz/cm^2;
- streamer probability ≈ 10^{-3}.

The beam intensity in the present tests was relatively low – around 150kHz. But it was already demonstrated in our previous tests of the WPC prototypes [1] that the chamber can operate up to 500 kHz/pad without essential deterioration of its performance.

The obtained parameters of the WPC satisfy with sufficient redundancy all requirements to the muon chambers in the outer region of the LHCb Muon System.

Acknowledgments.

The authors express their gratitude to the LHCb muon group helping in preparations of the beam tests at CERN. In particular, we are thankful to B. Schmidt, W. Riegler, T.Schneider, A.Kachtchouk who provided the data acquisition and beam trigger systems, the gas supply line, and other equipment needed in the test run. Many thanks to H.J. Hilke for permanent support of this work.

References.

1. B.Botchin et al. Wire Pad Chamber for LHCb Muon System. LHCb 2000-003 Muon. 14 Fev. 2000.

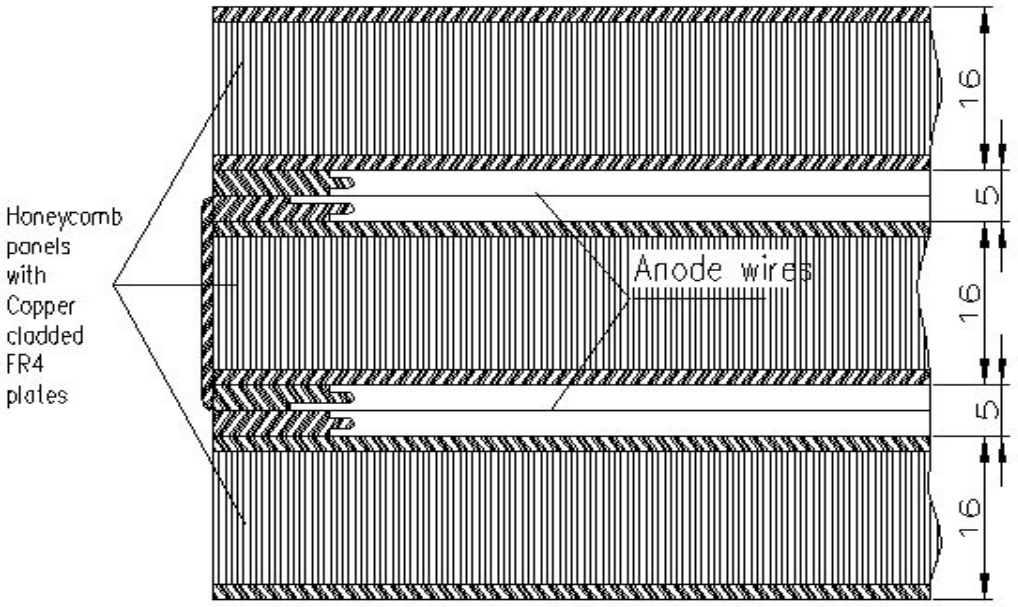

Figure 1a. Schematic view of WPC-7. Wire fixation geometry.

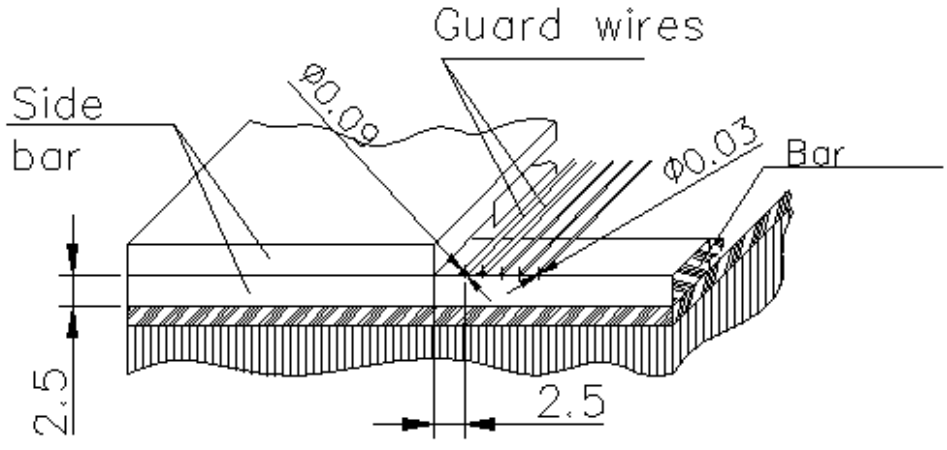

Figure 1b Schematic view of WPC-7. Guard wire geometry.

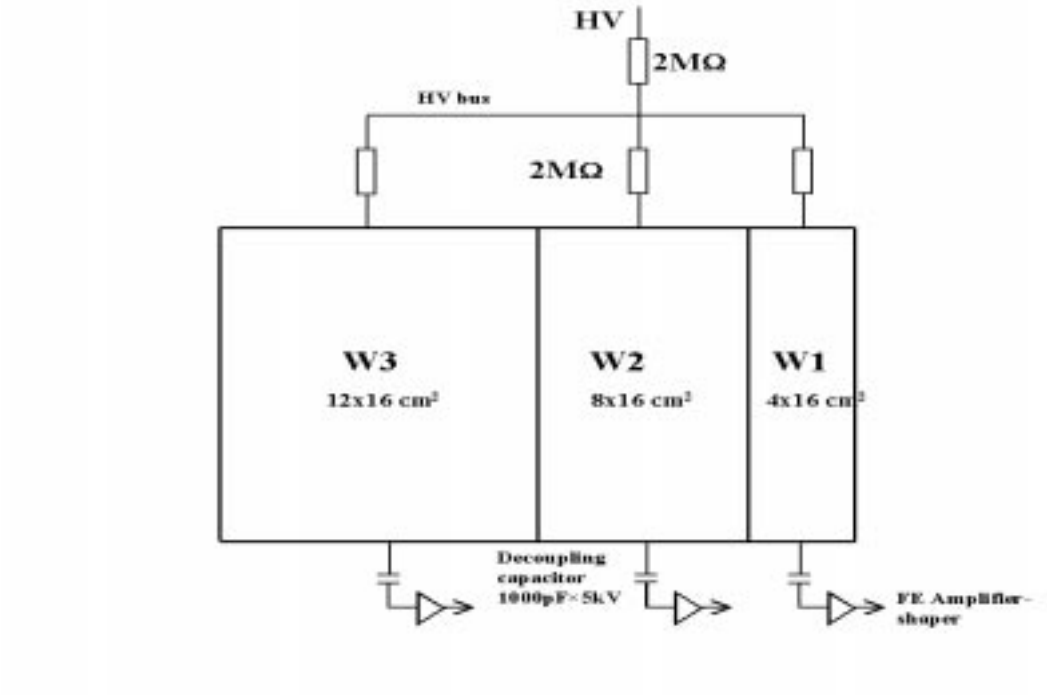

Figure 1c. Wire pads structure in WPC-7.

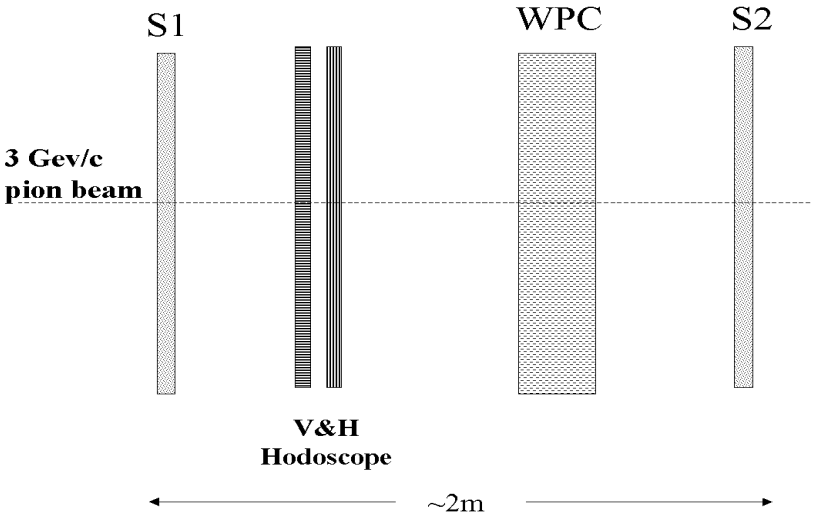

Figure 2. Experimental setup.
S1 – scintillator counter 15x15cm^2
S2 – scintillator counter 20x20cm^2
V&H Hodoscope – 8x8 scintillator counters 1x8cm^2

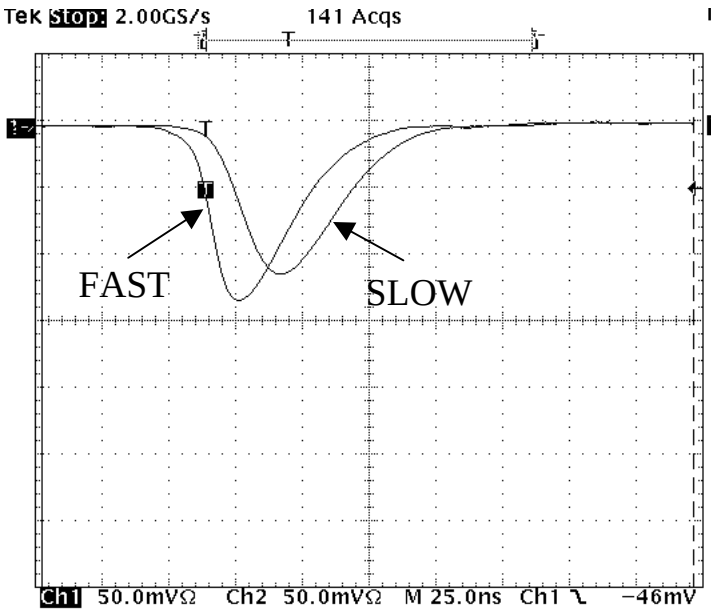

Figure 3a Averaged signals at the output of the Main Amplifier. Pad W1 (4x16cm^2).

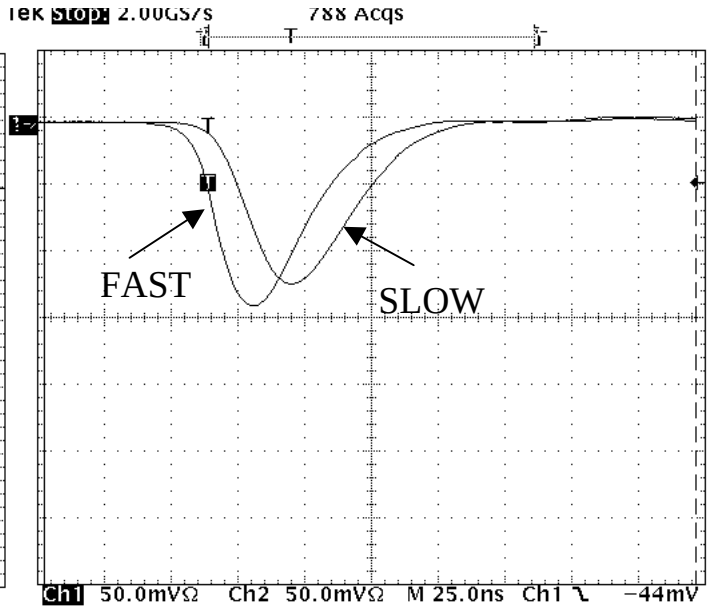

Figure 3b Averaged signals at the output of the Main Amplifier. Pad W3 (12x16cm^2).

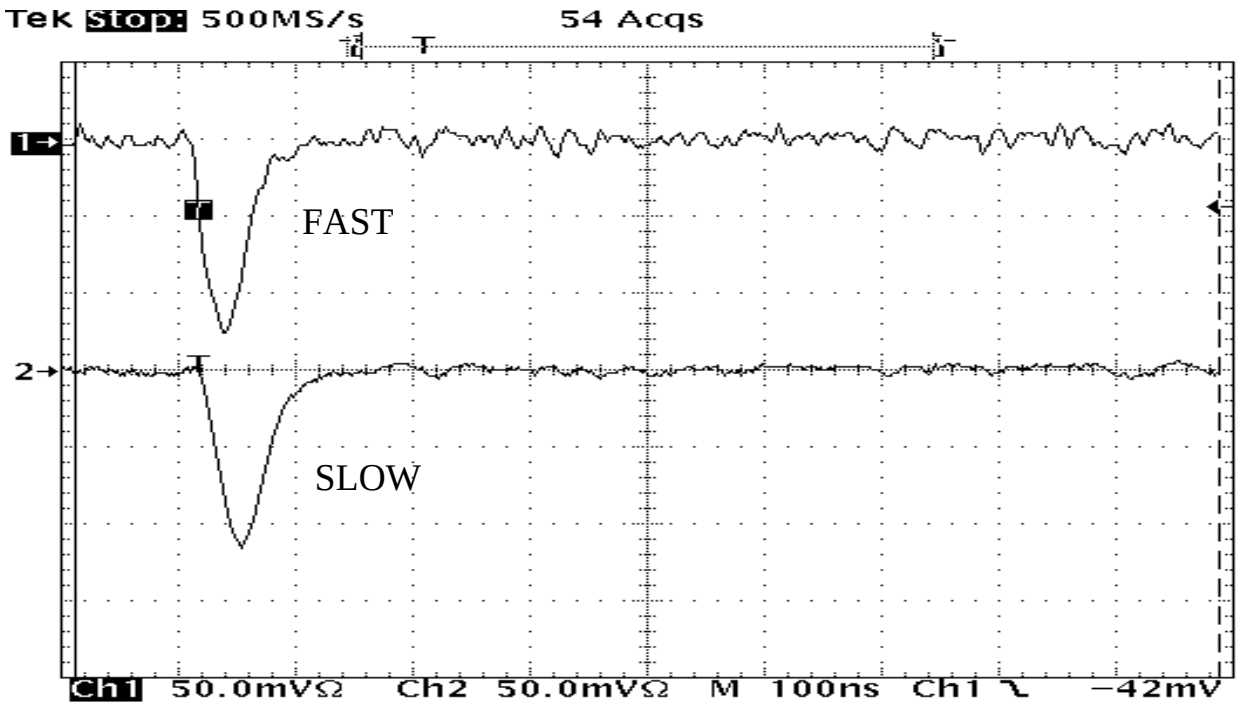

Figure 3c Display of single signals in SLOW and FAST channels at the output of the Main Amplifier.

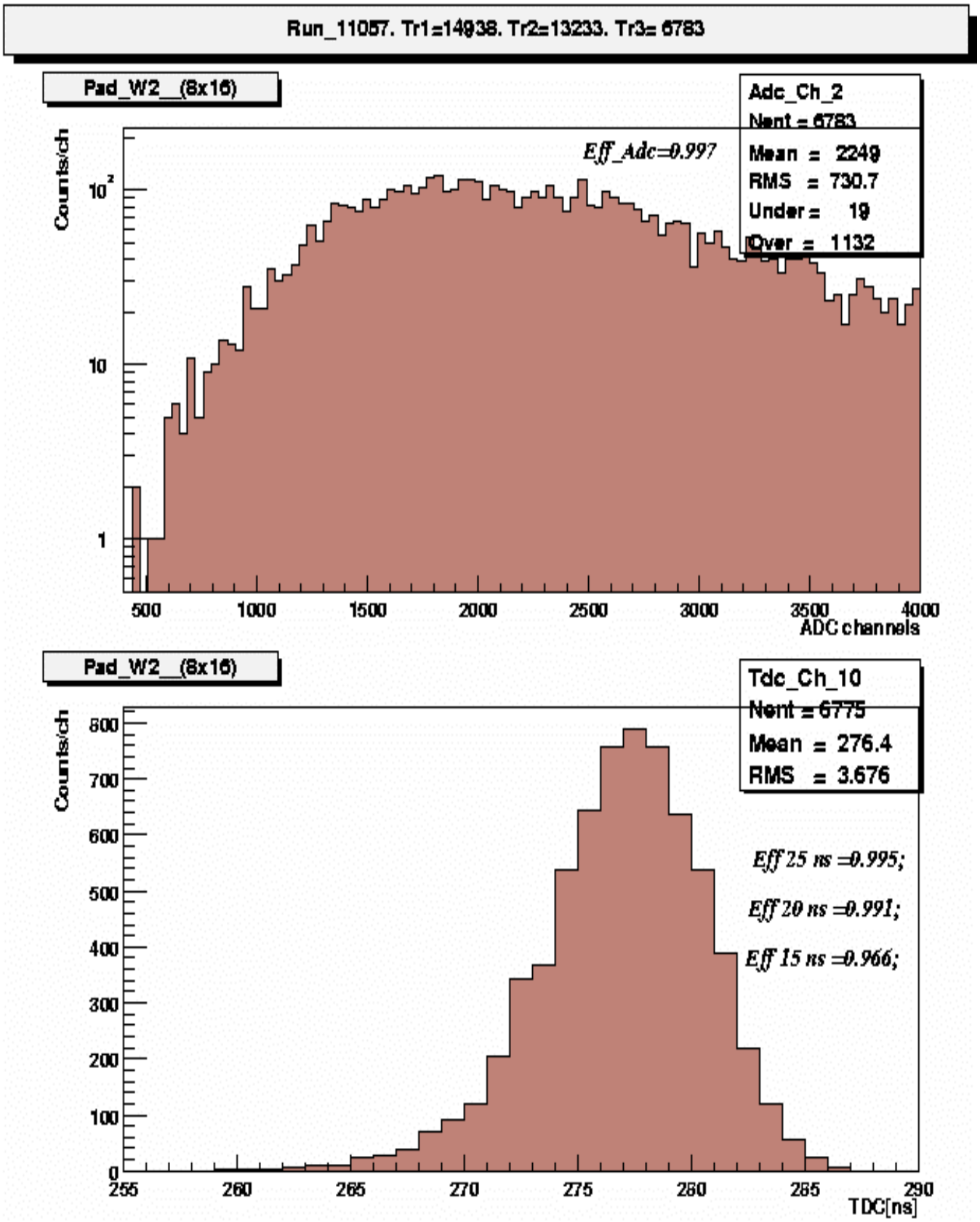

Figure 4. ADC and TDC spectra of the signals from pad W2 (8x16 cm^2) measured at the nominal HV=3.15 kV. The ADC pedestal is on channel 260. The discriminator threshold is set at Th=35mV. The beam spot is selected by hodoscope counters to be inside the pad size.

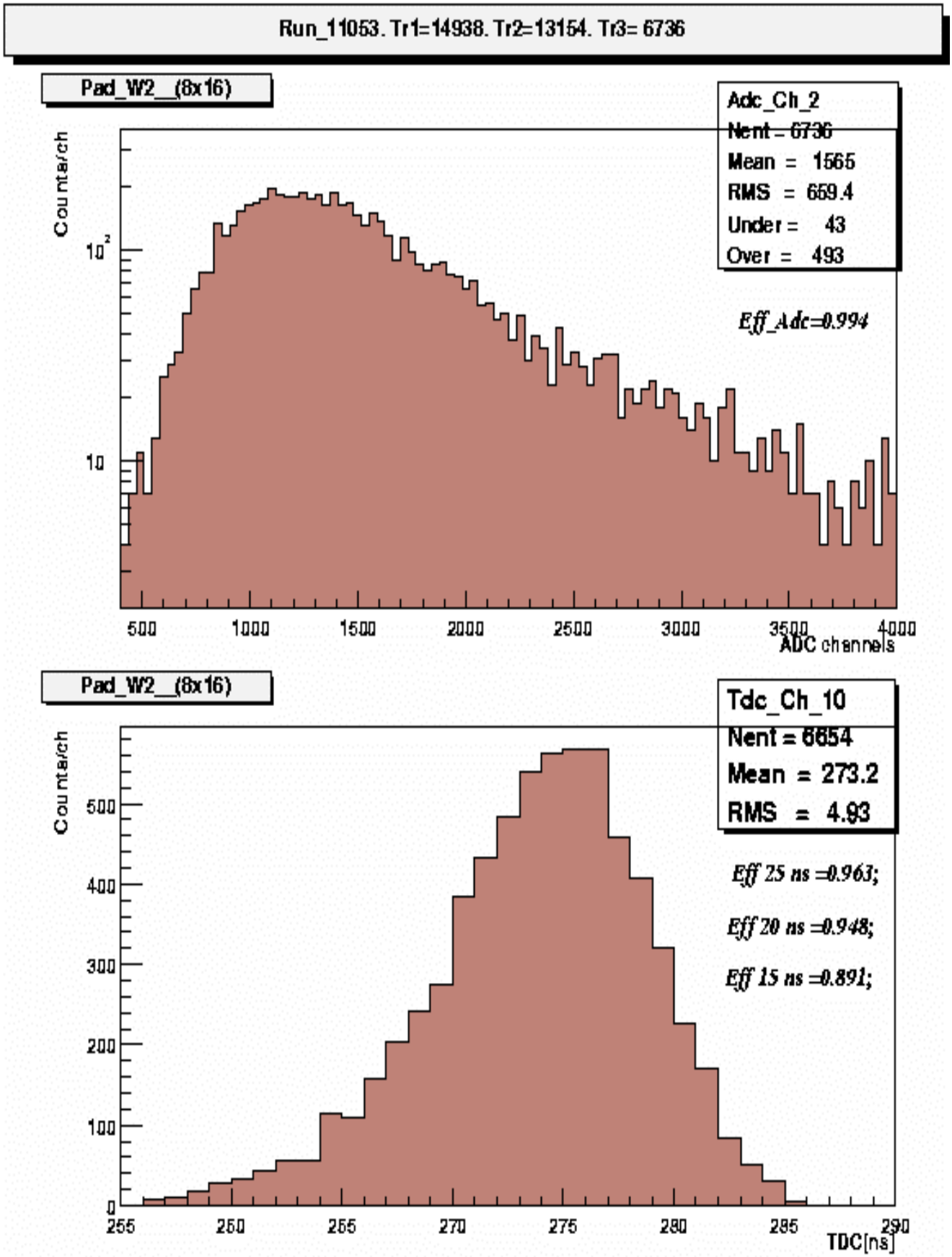

Figure 5. ADC and TDC spectra of the signals from pad W2 measured at HV=3.05kV, Th=35mV.

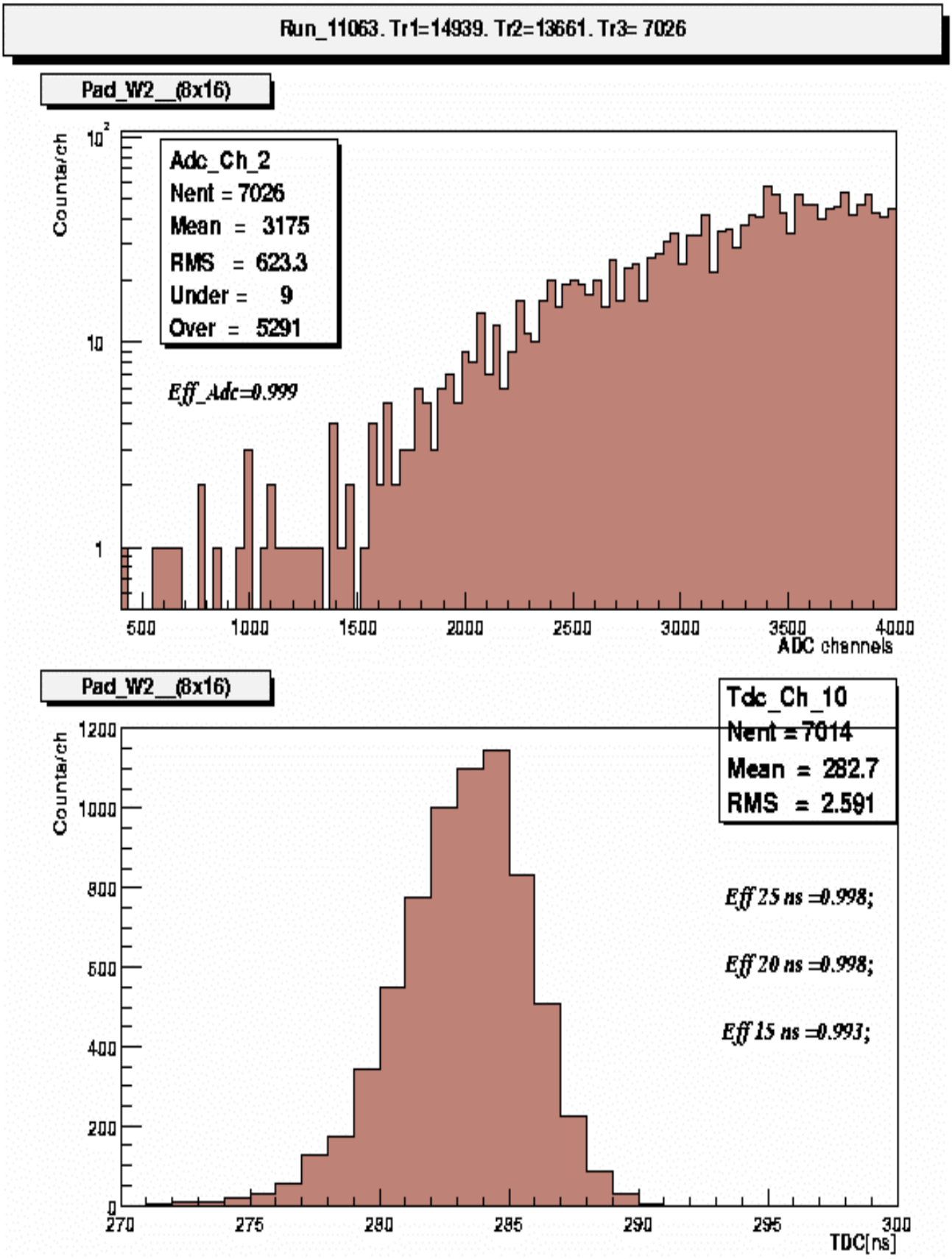

Figure 6. ADC and TDC spectra of the signals from pad measured at HV=3.30 kV, Th=35mV.

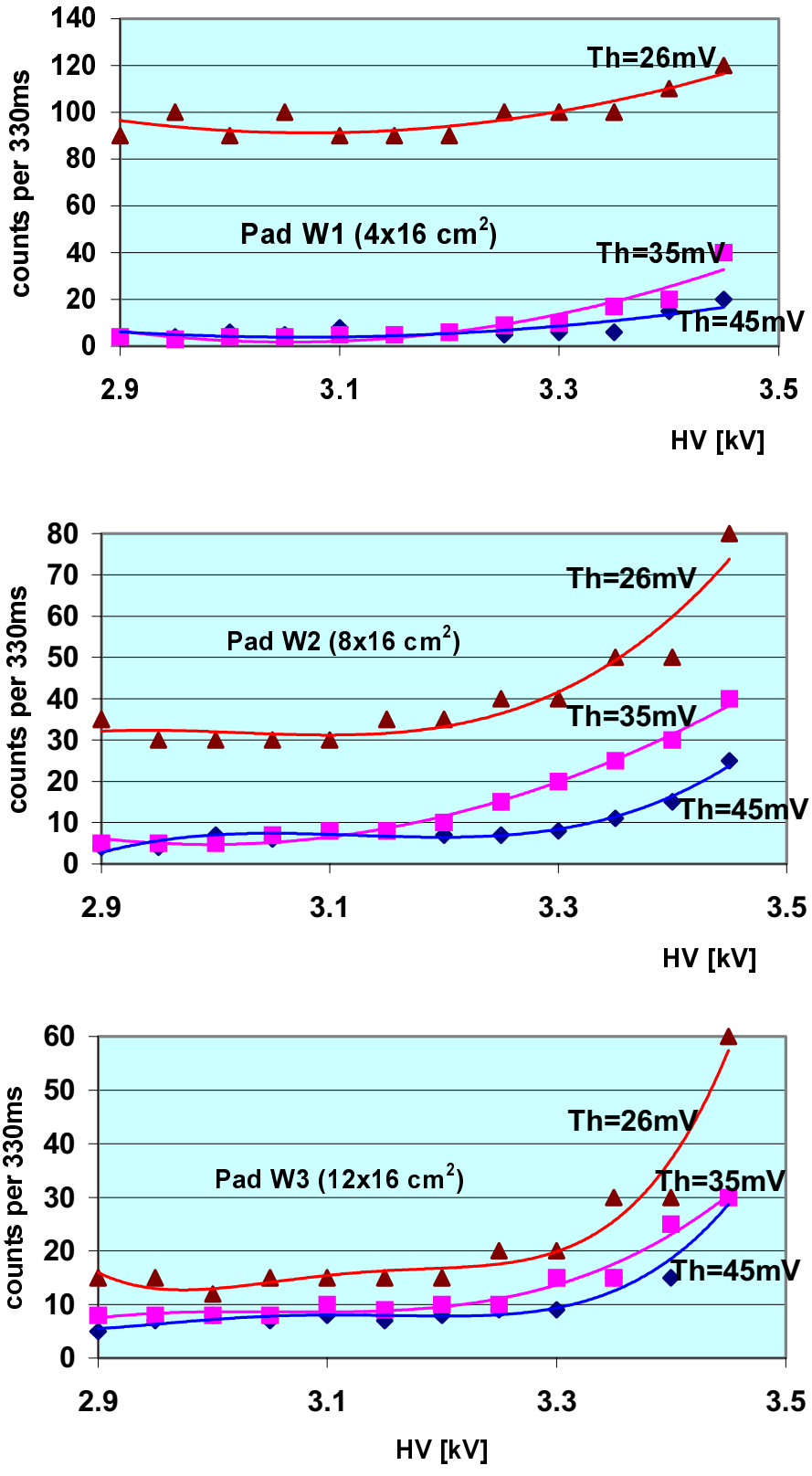

Fig 7. Noise counting rates vs HV for various discriminator thresholds

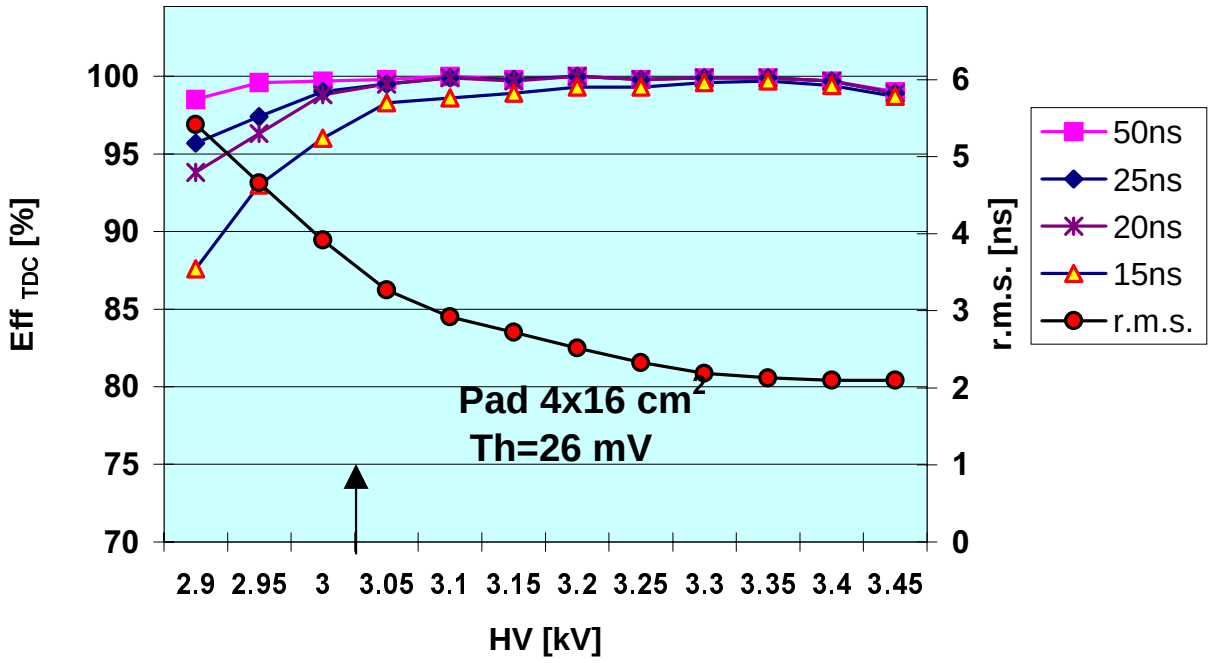

Figure 8a. Efficiency in various time windows and time resolution for pad W1 (4x16 cm2), Th=26mV. The arrow indicates the position of HV $_{nominal}$

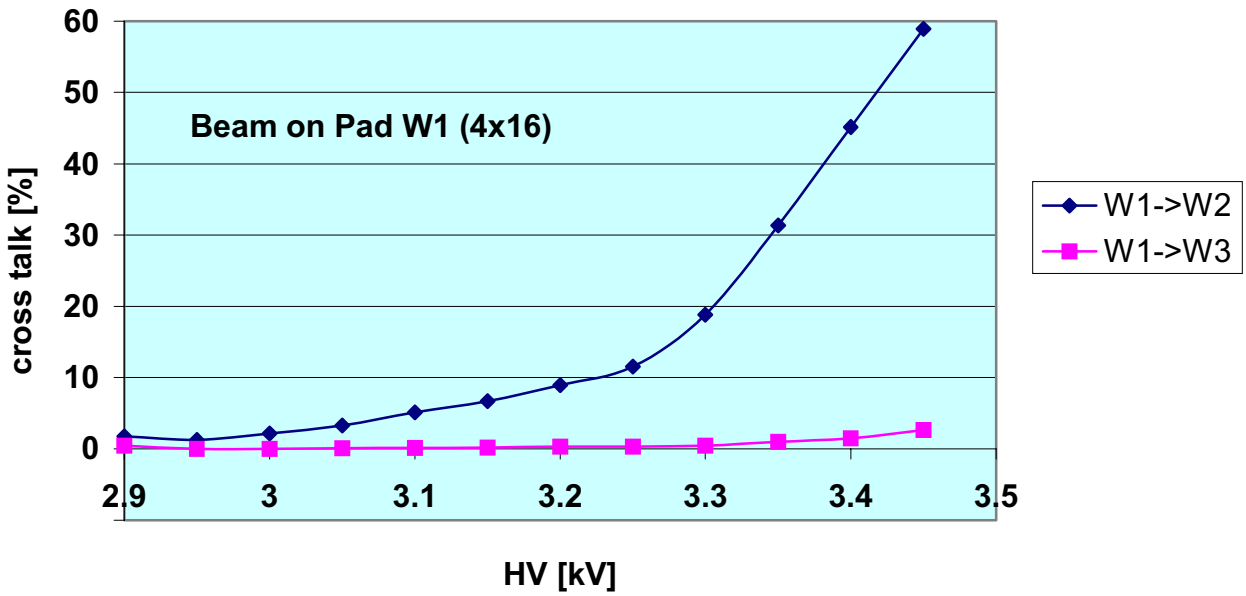

Figure 8b. Probability to detect signals from pads W2 and W3 in 300 ns time window with the beam focused on pad W1, Th=26mV.

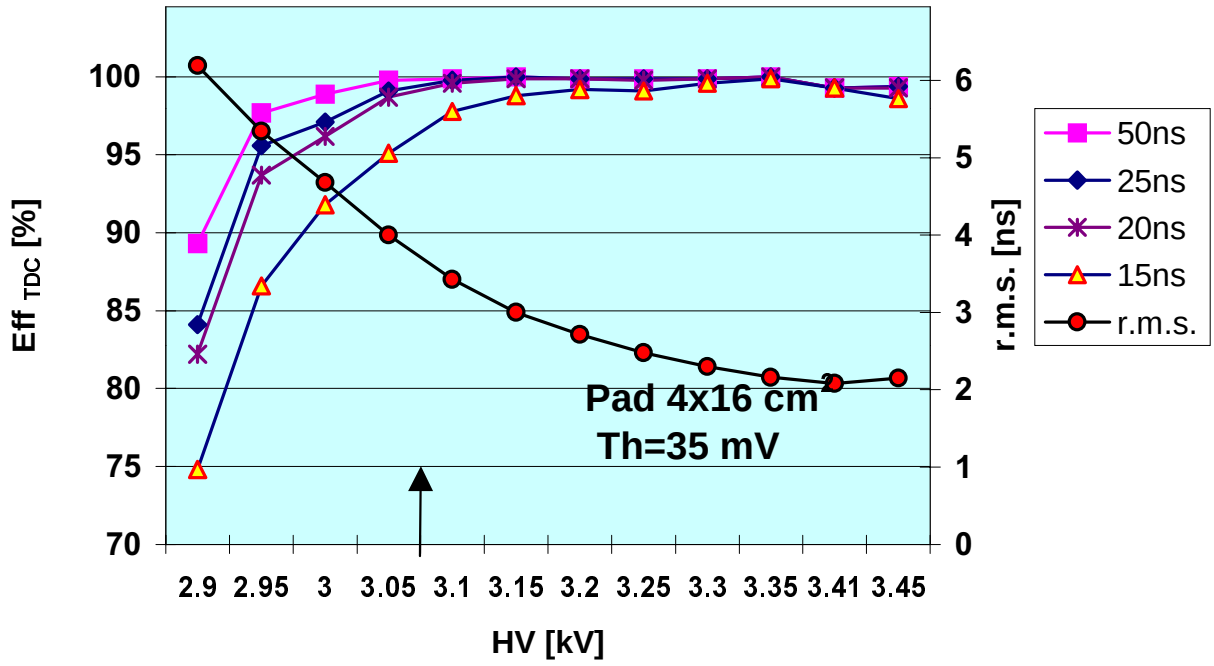

Figure 9a. Efficiency in various time windows and time resolution for pad W1 (4x16 cm^2), Th=35mV.

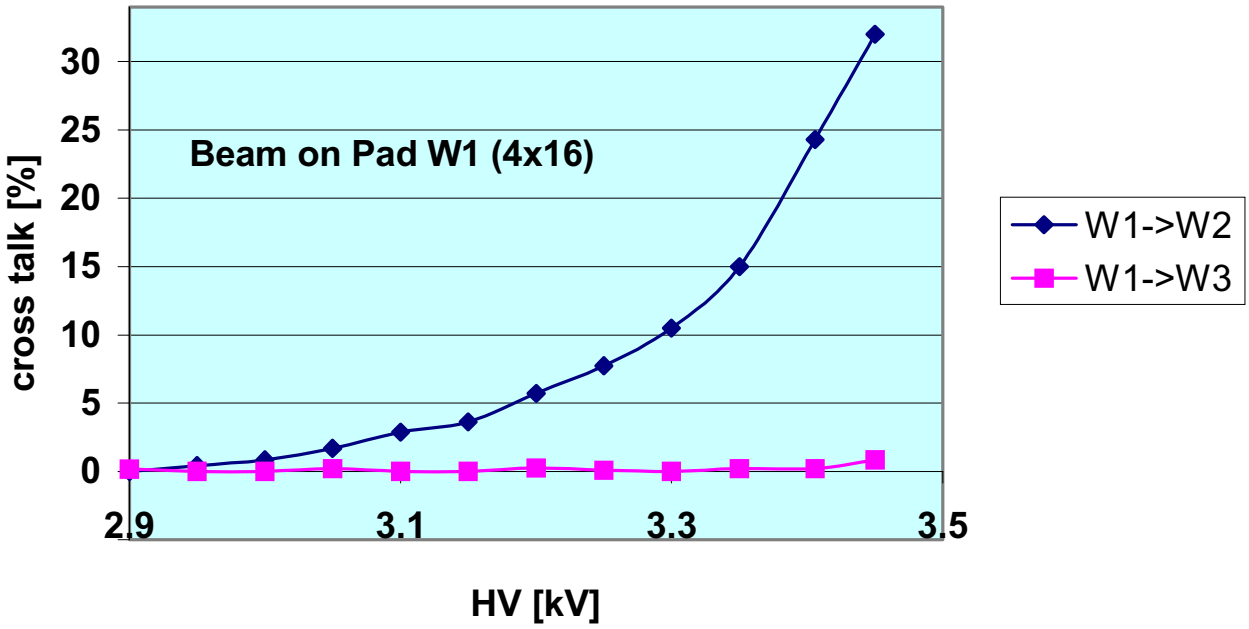

Figure 9b. Probability to detect signals from pads W2 and W3 in 300 ns time window with the beam focused on pad W1, Th=35mV.

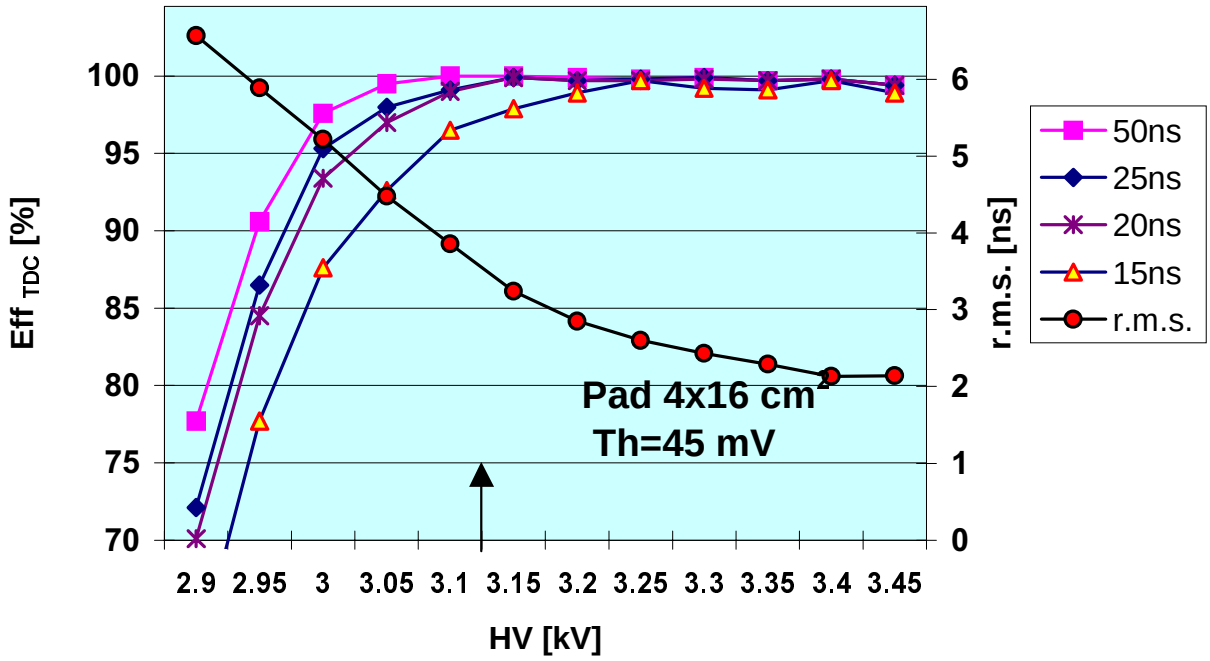

Figure 10a. Efficiency in various time windows and time resolution for pad W1 (4x16 cm2), Th=45mV.

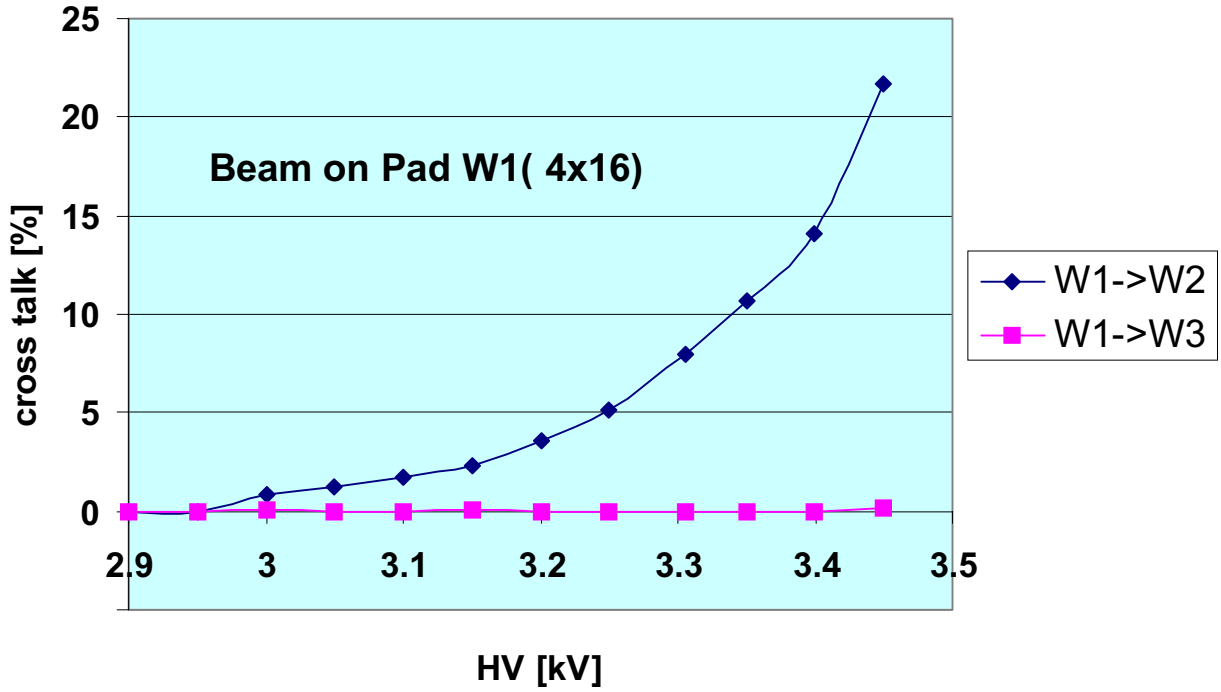

Figure 10b. Probability to detect signals from pads W2 and W in 300 ns time window with the beam focused on pad W1, Th=45mV.

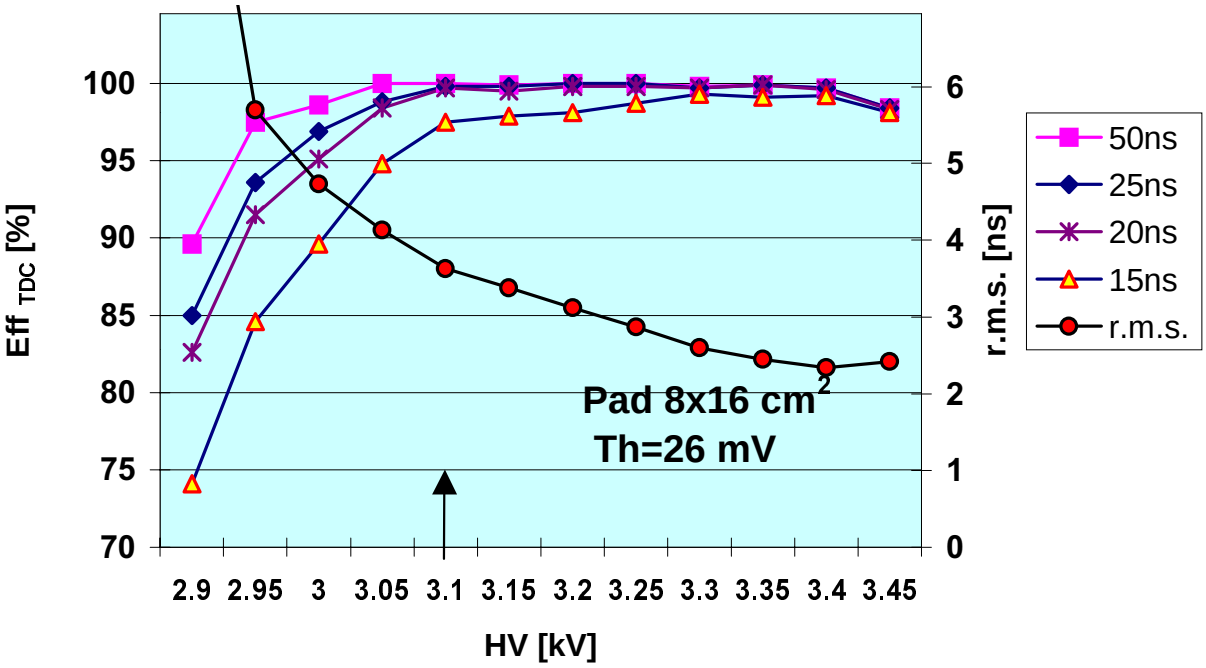

Figure 11a. Efficiency in various time windows and time resolution for pad W2 (8x16 cm2), Th=26mV.

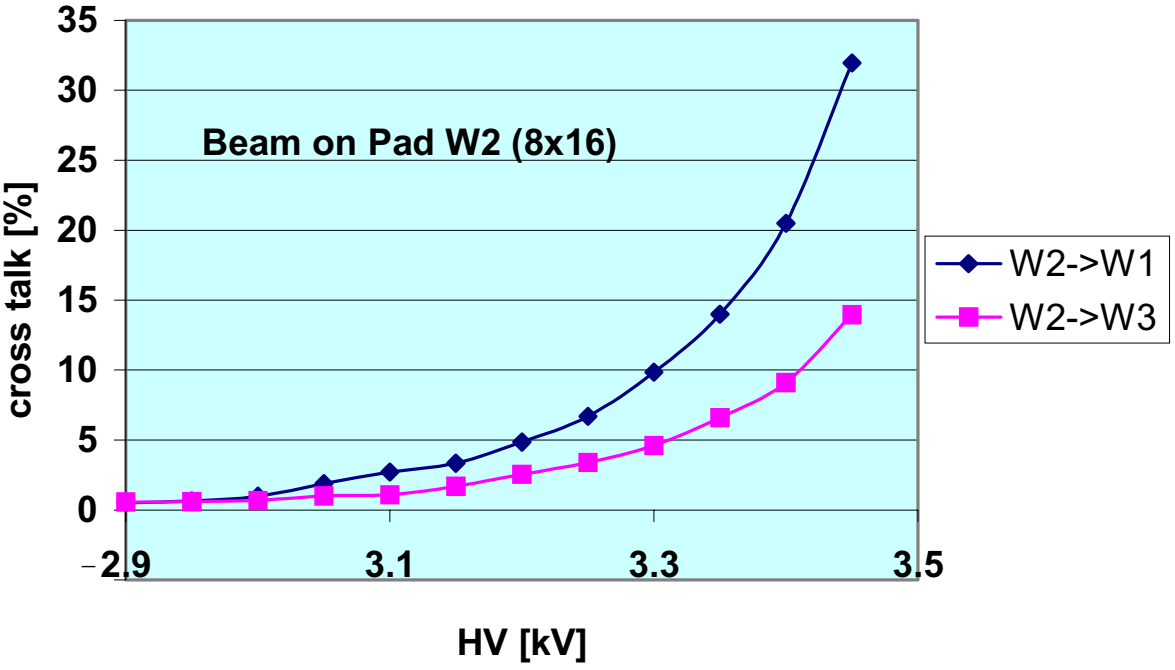

Figure 11b. Probability to detect signals from pads W1 and W3 in 300 ns time window with the beam focused on pad W2, Th=26mV.

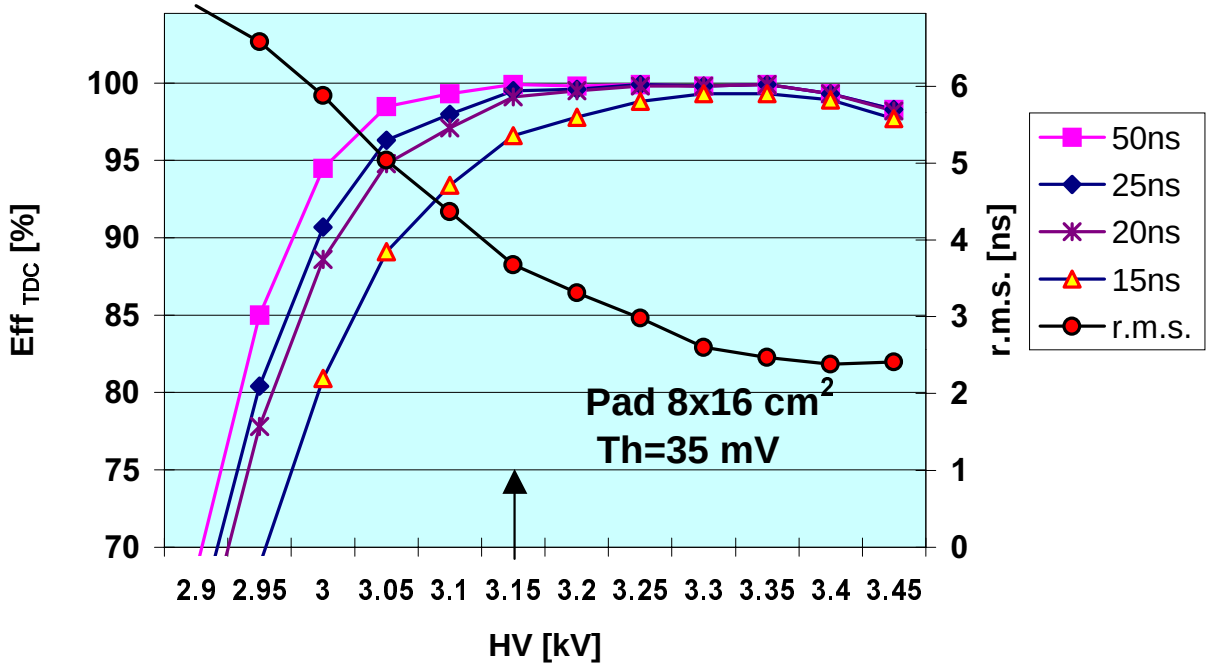

Figure 12a. Efficiency in various time windows and time resolution for pad W2 (8x16 cm2), Th=35mV.

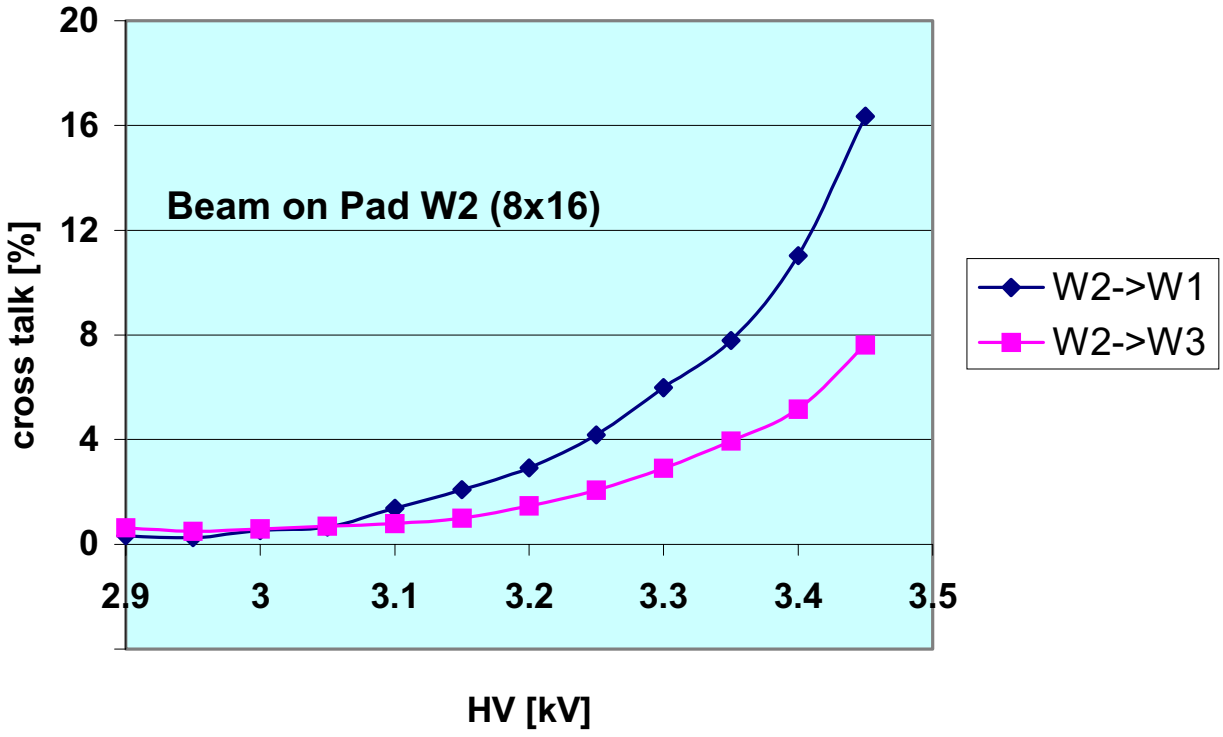

Figure 12b. Probability to detect signals from pads W1 and W3 in 300 ns time window with the beam focused on pad W2, Th=35mV.

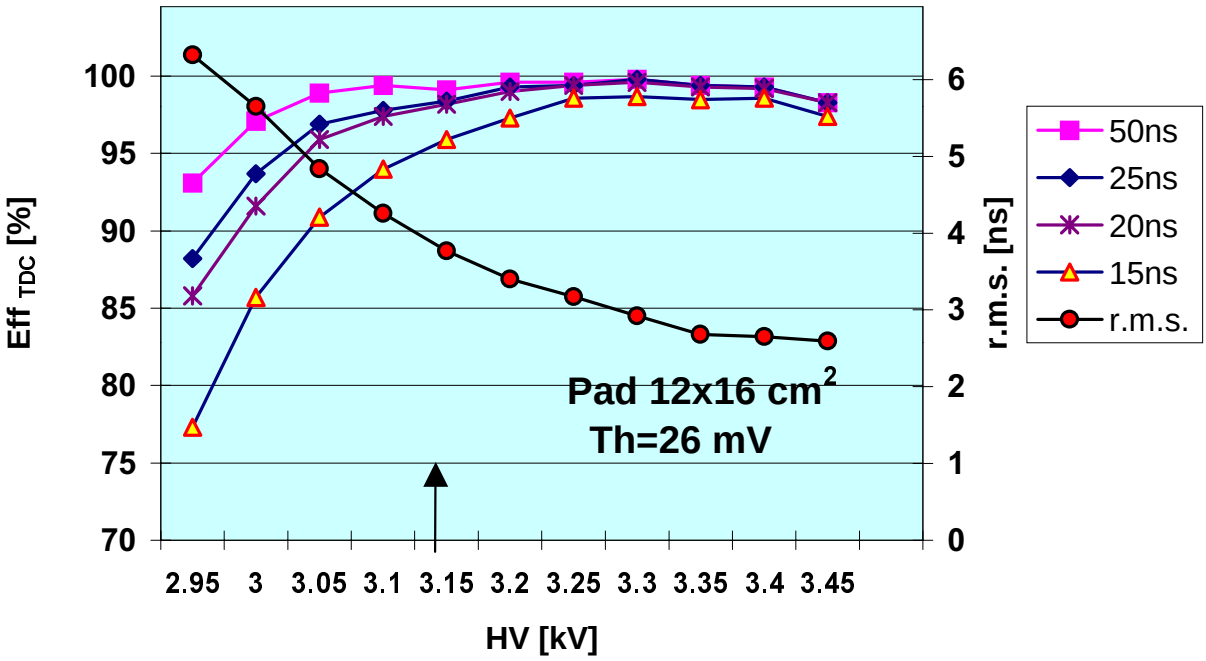

Figure 13a. Efficiency in various time windows and time resolution for pad W3 (12x16cm^2), Th=26mV.

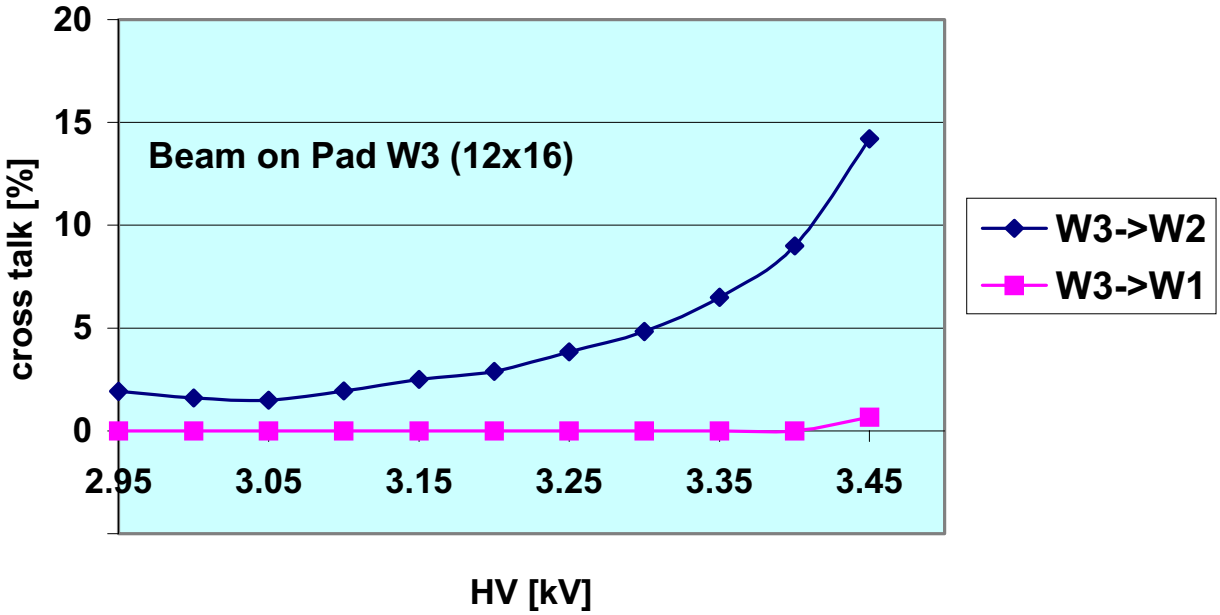

Figure 13b. Probability to detect signals from pads W1 and W2 in 300 ns time window with the beam focused on pad W3, Th=26mV.

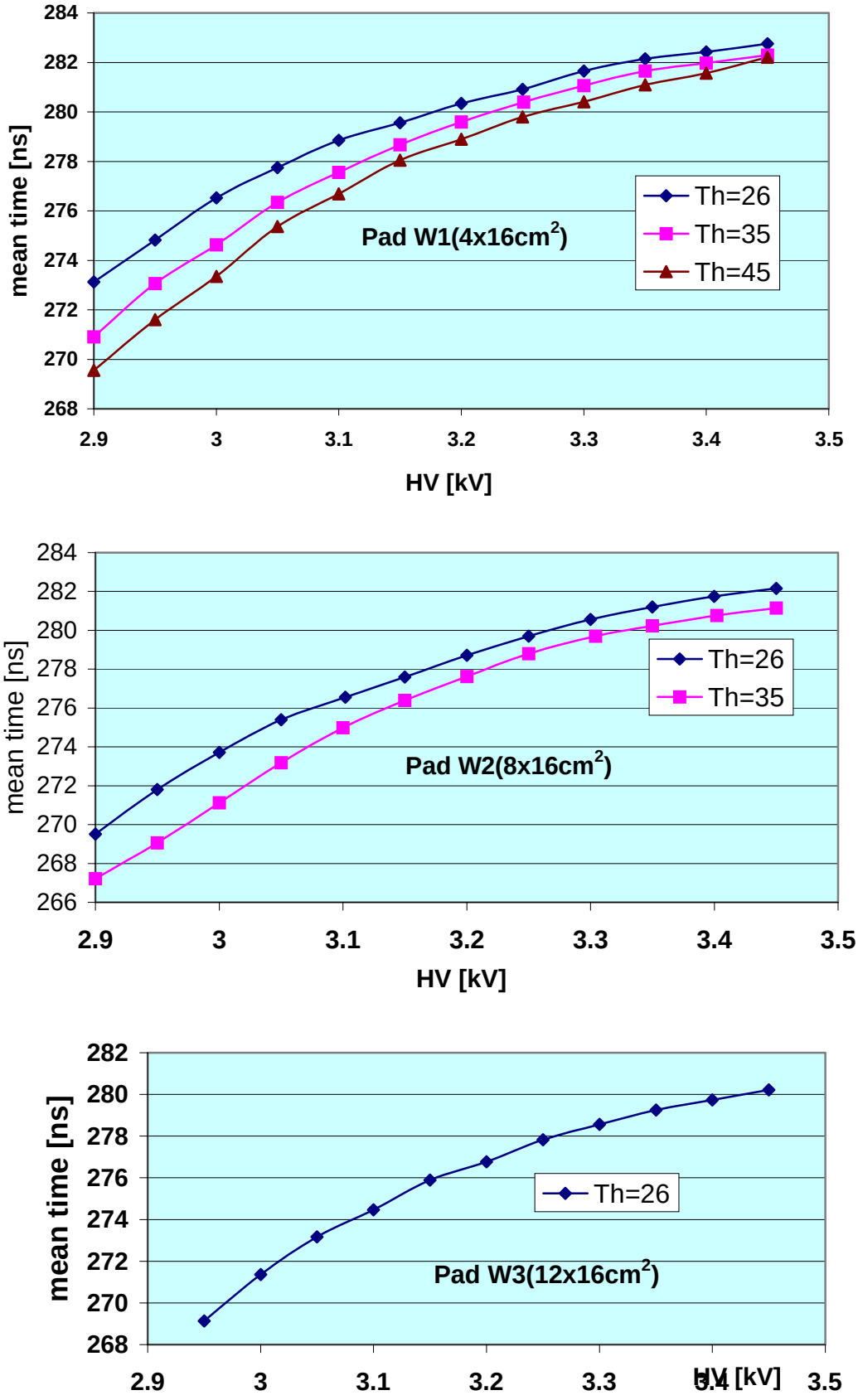

Figure 14. TDC mean time vs HV for various pad sizes and thresholds.

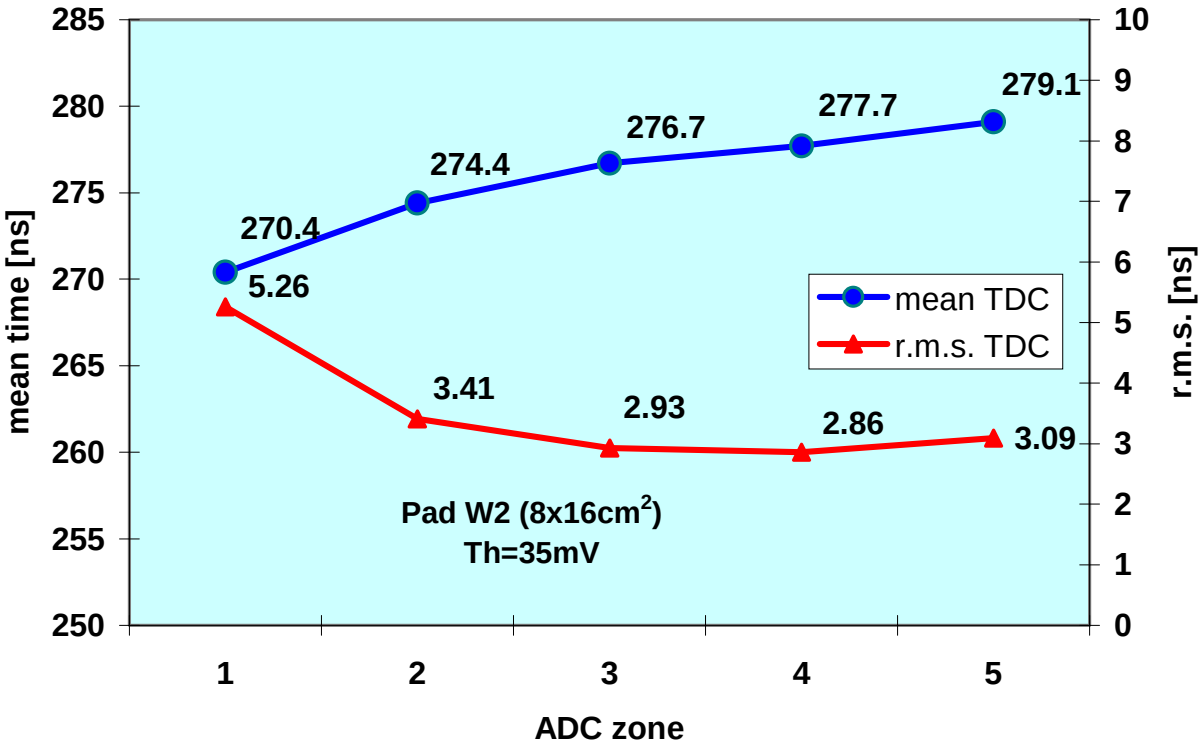

zone	channels	events
1	400..1000	144
2	1000..2000	2403
3	2000..3000	2576
4	3000..4000	1067
5	overflow	1254

Figure 15. TDC mean and r.m.s.values vs ADC amplitude. Pad W2 (8x16 cm^2).
Th=35 mV, HV=3.15 kV.

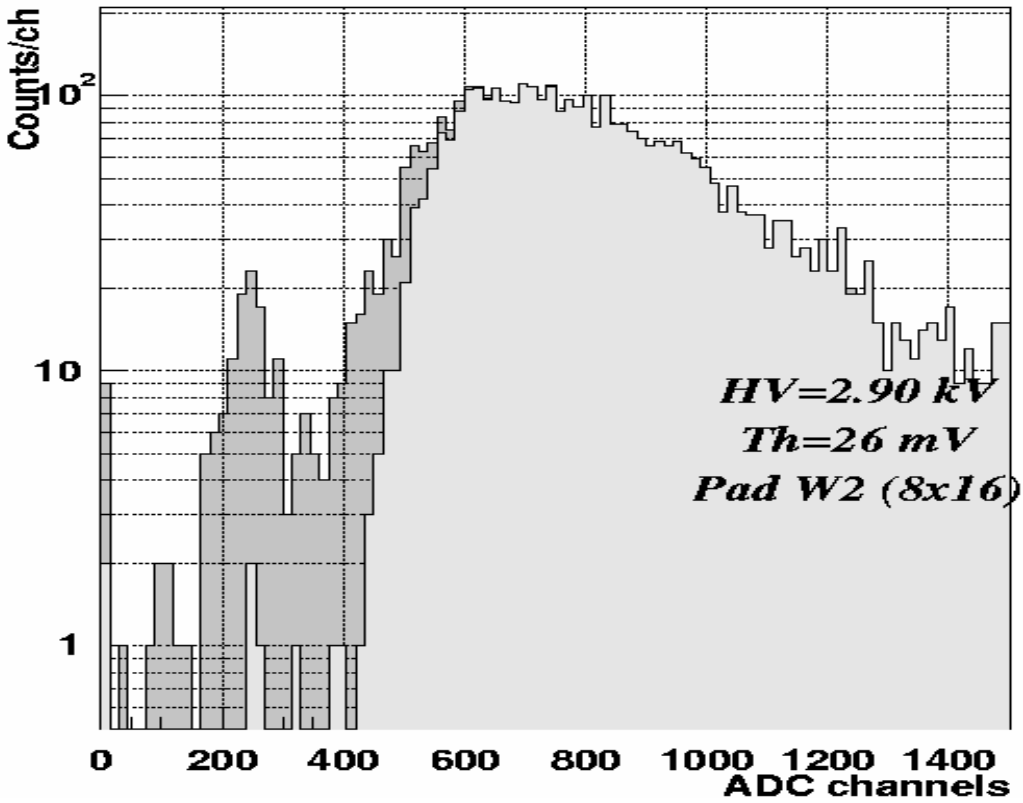

Figure 16a. ADC spectra with and without requirement of the signals in the 30ns time window in the TDC channel. Pad W2 (8x16 cm^2), Th=26 mV, HV=2.9 kV.

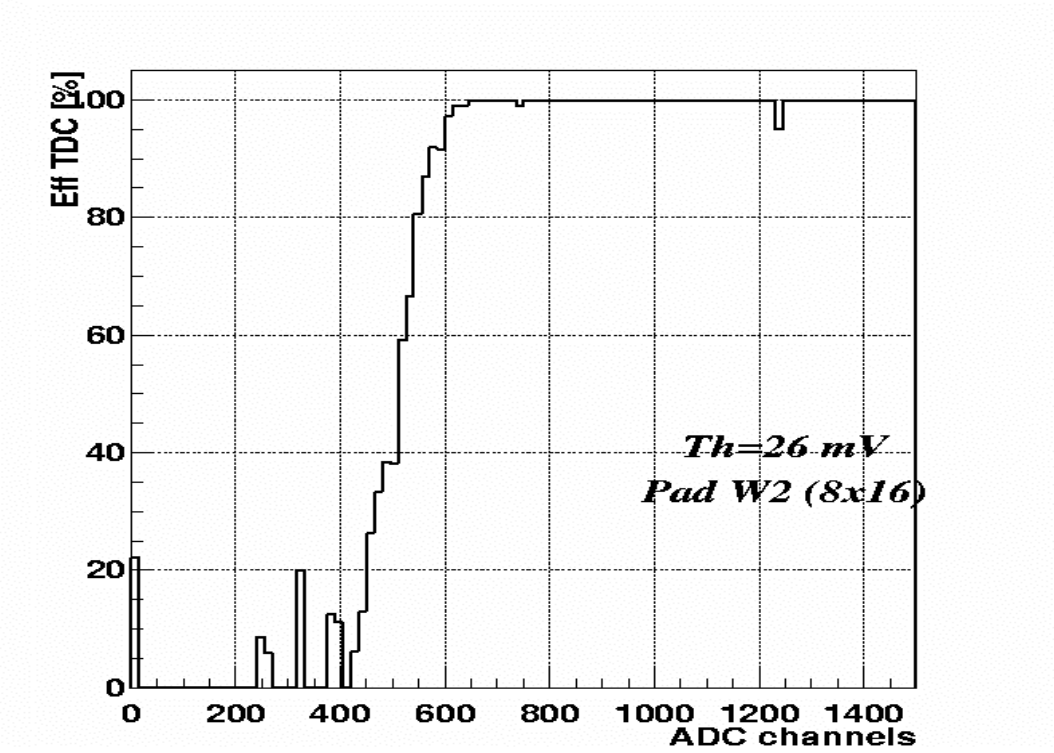

Figure 16b. Efficiency of the TDC channel (30 ns window) vs signal amplitude measured in ADC channel. Pad W2 (8x16 cm^2), Th=26 mV.

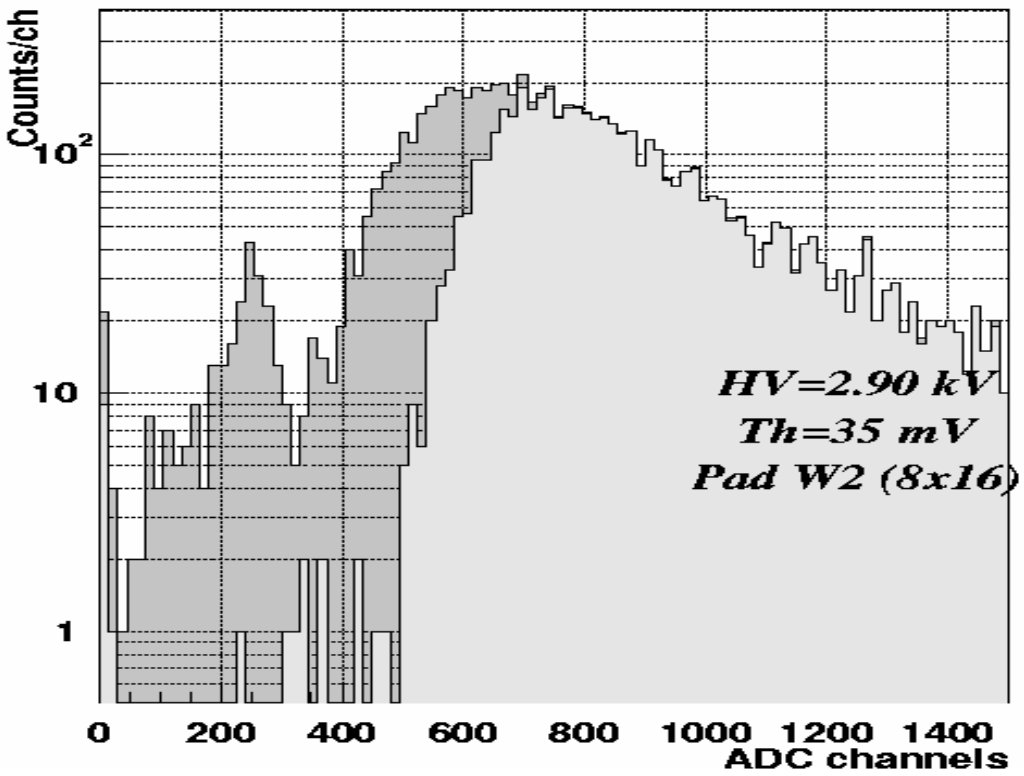

Figure 17a. ADC spectra with and without requirement of the signals in the 30 ns time window in the TDC channel.
Pad W2 (8x16 cm^2), Th=35 mV, HV=2.9 kV.

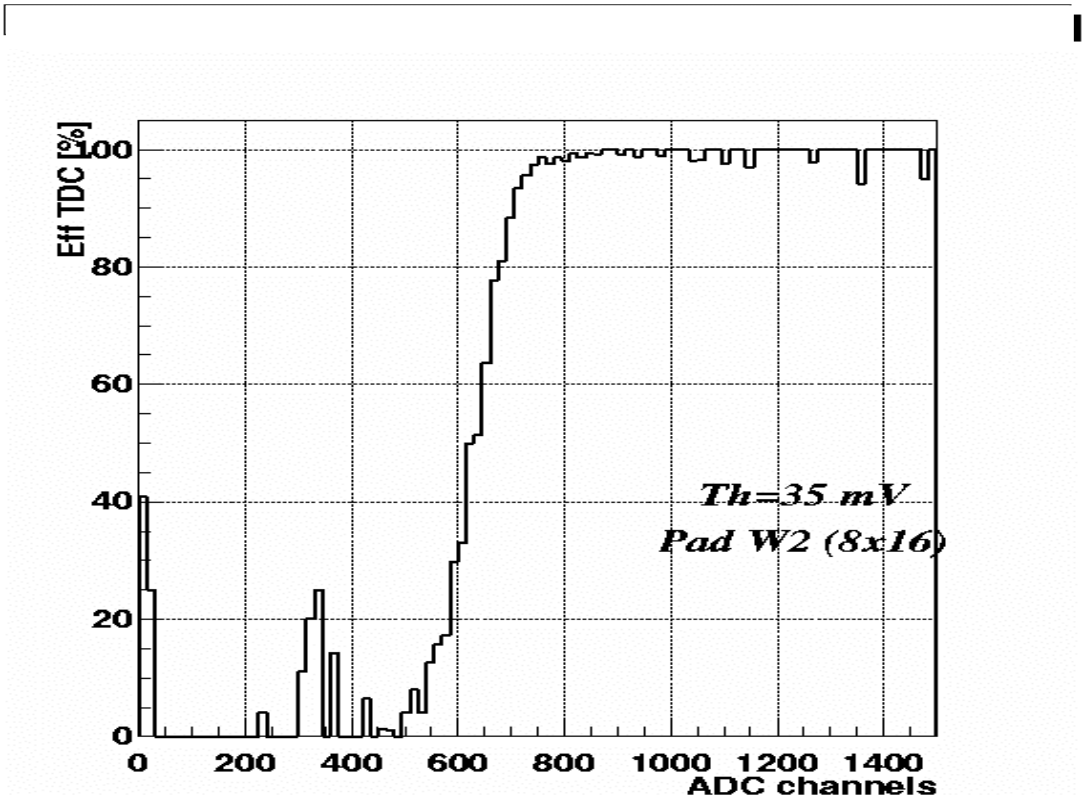

Figure 17b. Efficiency of the TDC channel (30 ns window) vs signal amplitude measured in ADC channel. Pad W2 (8x16 cm^2), Th=35 mV.

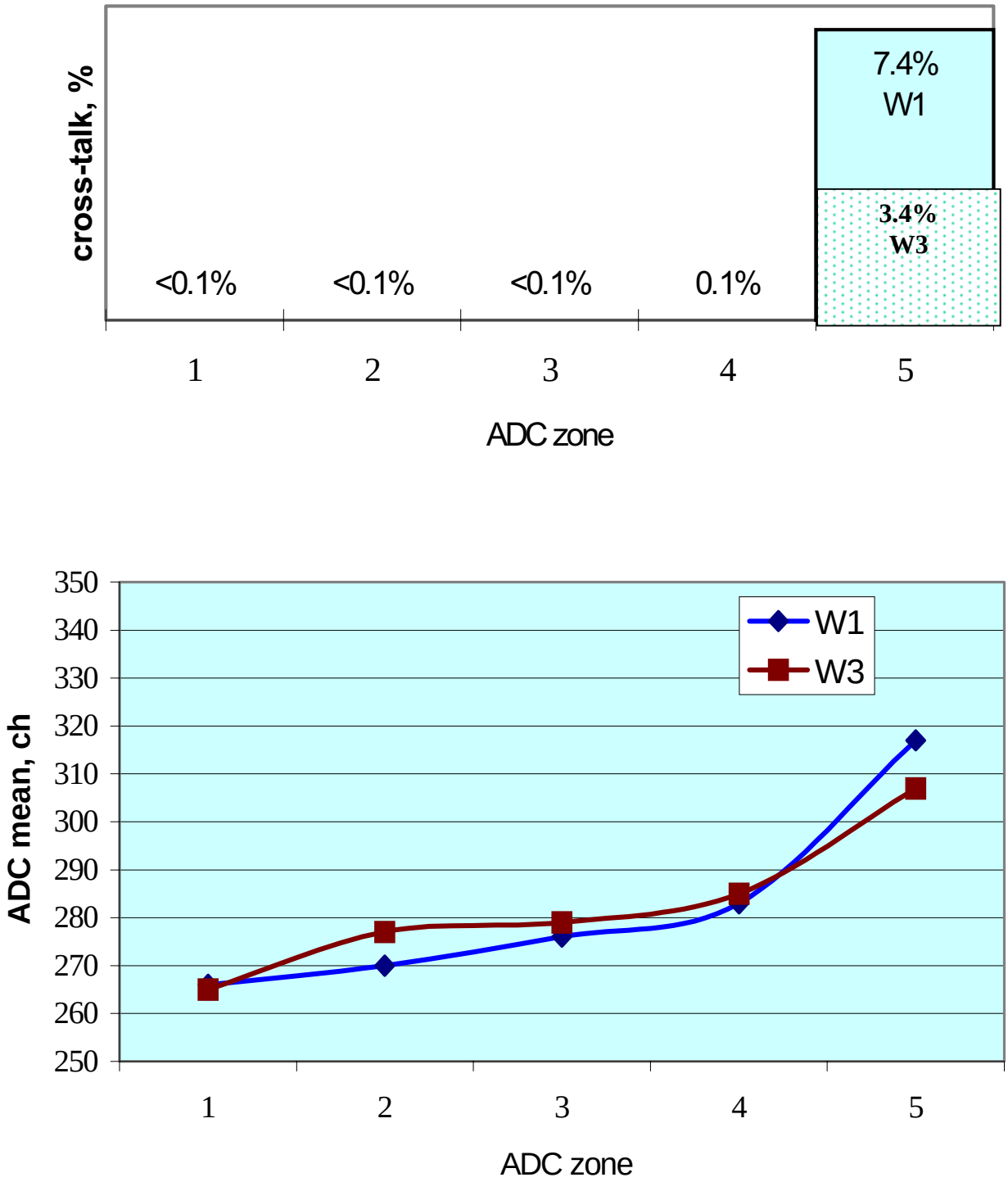

Figure 18. Probability of the TDC cross-talk signals and the ADC means in the W1 and W3 channels vs ADC amplitude in the W2 channel. Beam spot is within pad W2 (8x16 cm^2), HV=3.15 kV, Th=35 mV.
The definition of the ADC zones is as in Figure 15.

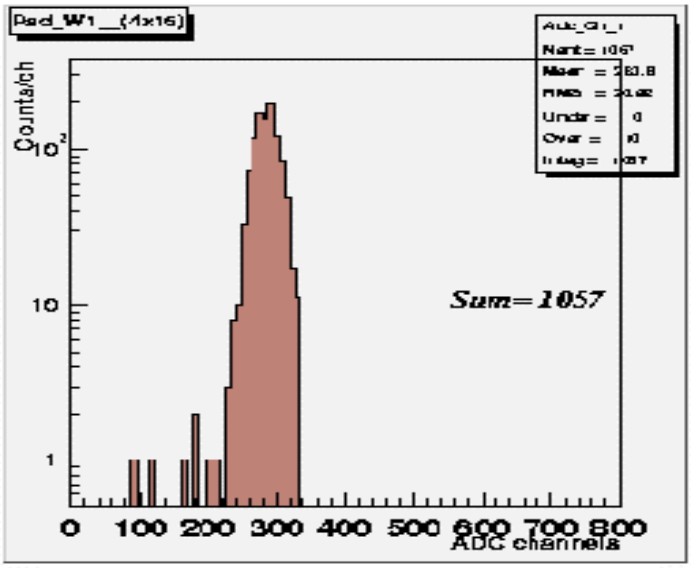

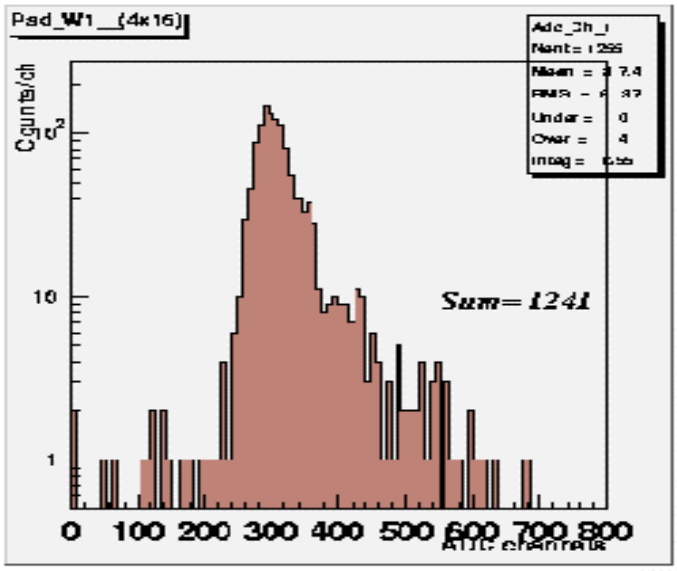

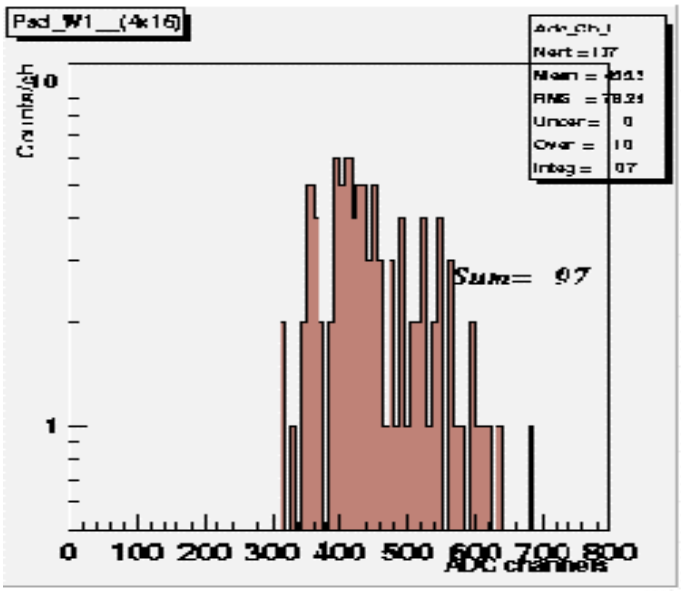

Figure 19. ADC spectrum in the W1-channel for various selections of amplitudes in the W2-channel. The beam spot is on the W2 pad, HV=3.15kV, Th=35 mV.

a) Selected events are in the ADC zone 4 of the W2-channel.
b) Selected events are in the ADC zone 5 (overflow) of the W2-channel
c) Coincidence with the TDC cross-talk signals in the W1-channel.

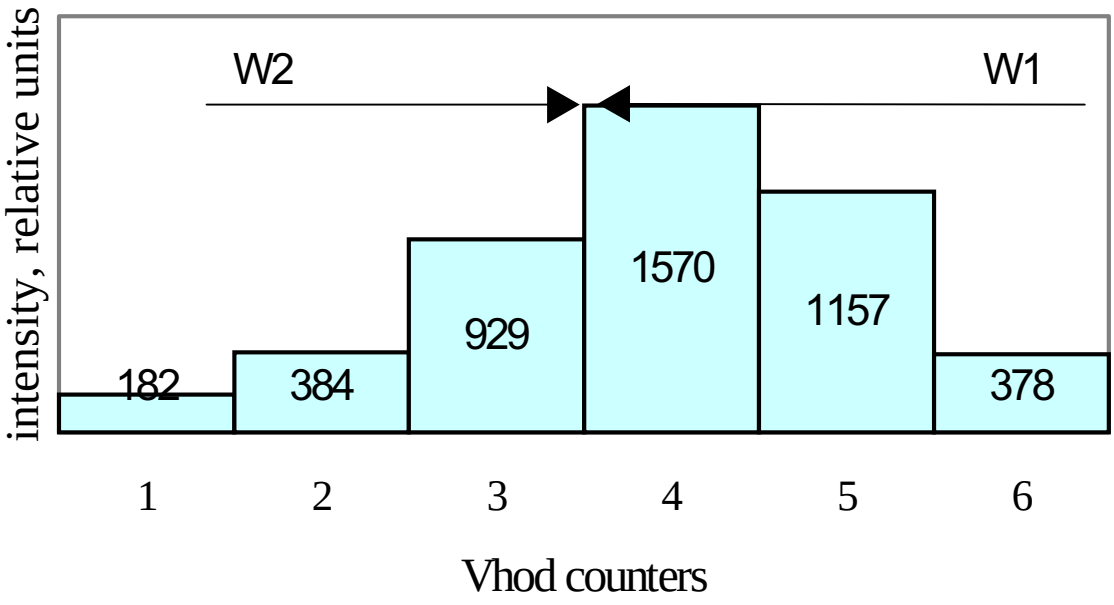

Figure 20a. Beam profile as measured with Vhod counters.

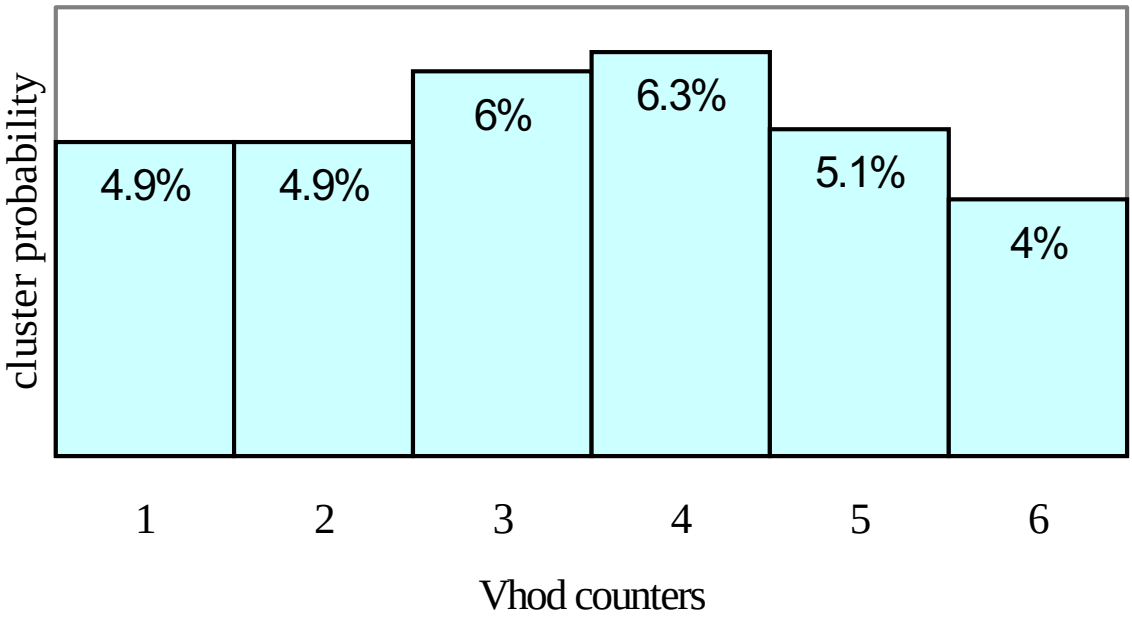

Figure 20b. Double plus triple cluster probability for various positions of the beam spot. HV=3.15kV. Th=35 mV.
The width of each Vhod counter is 1 cm. The border between pads W2 and W1 corresponds to the border between Vhod 3 and Vhod 4.

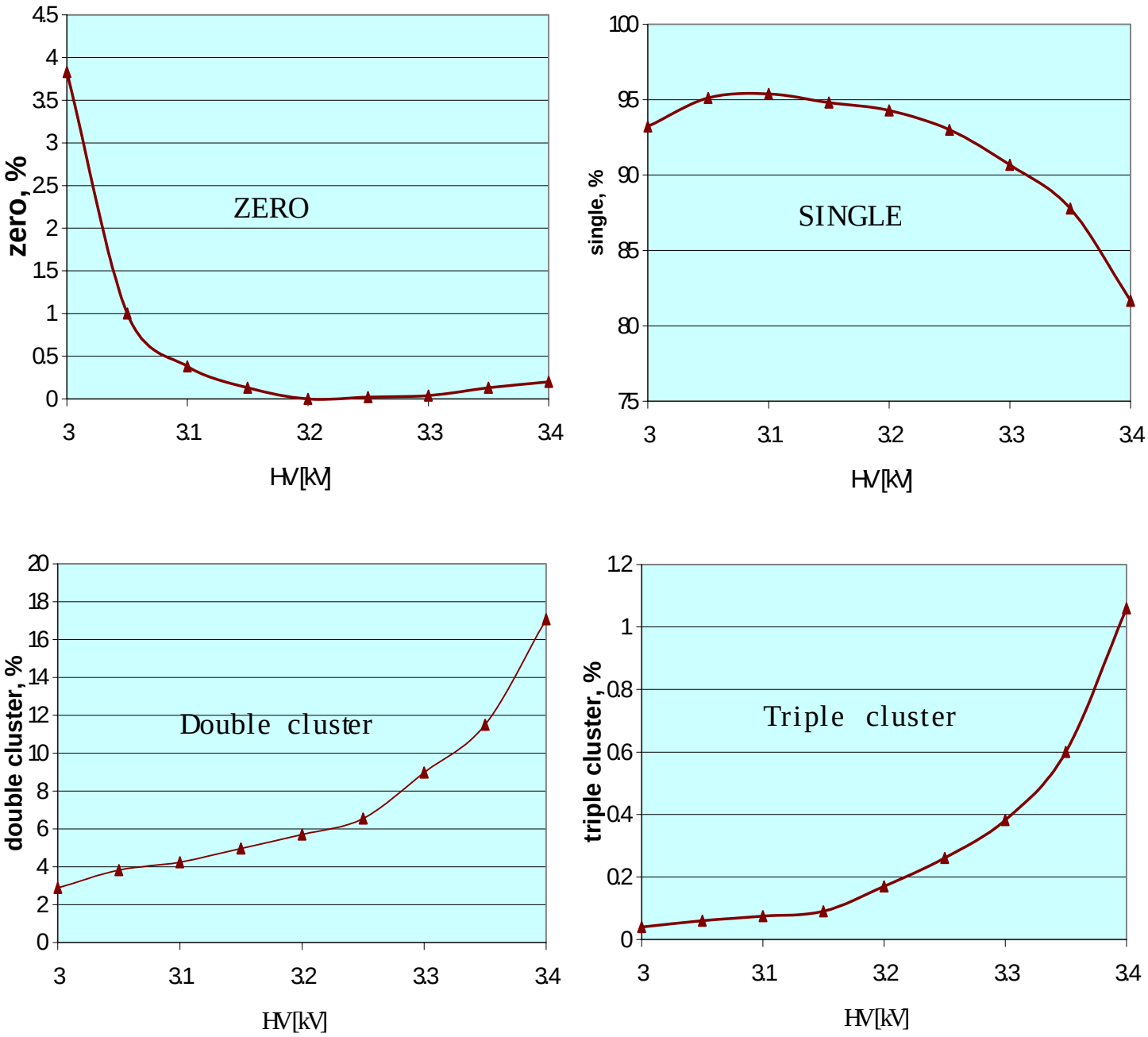

Figure 21. Cluster size distribution vs HV. Measurements with “wide” beam profile shown in Figure 20a. Th=35 mV.